TECHNISCHE UNIVERSITÄT DRESDEN

Higher Order Studies of Polarization Effects in $W^{\pm}Z$ Production at the LHC With Sherpa

Bachelorarbeit
zur Erlangung des Hochschulgrades
Bachelor of Science
im Bachelor-Studiengang Physik

vorgelegt von

Johannes Nikolas Liebig
geboren am 23.04.2002 in Dresden

Institut für Kern- und Teilchenphysik
Fakultät Physik
Bereich Mathematik und Naturwissenschaften
Technische Universität Dresden

12.02.2024

Eingereicht am 12. Februar 2024

1. Gutachter: Dr. Frank Siegert
2. Gutachter: Prof. Dr. Arno Straessner

Abstract

Event generators are an important connector between experimental and theoretical particle physics. It is crucial that they can simulate every particle interaction described by the Standard Model of particle physics and beyond. In the newest beta version of Sherpa 3.0.0, a fully-multipurpose hadronic event generator, the polarization states of intermediate vector bosons can be simulated. The matrix element generator MadGraph, a multi-purpose parton level generator, is also able to simulate these polarization states, so the results for the $W^{\pm}Z$-production can be compared between both simulation programs. Another way to verify that Sherpa can simulate the effects of vector boson polarization, investigating theoretical peculiarities like the radiation amplitude zero effect, where the differential cross-section is equal to zero for a specific observable, is reasonable.
In many models discussing physics beyond the Standard Model, values of coupling parameters are tweaked which can impact polarization effects. Thus, if the simulation results differ from Standard Model expectations, the choice which of these model is correct can be limited.

Kurzdarstellung

Eventgeneratoren sind ein bedeutendes Bindeglied zwischen experimenteller und theoretischer Teilchenphysik. Es ist sehr wichtig, dass sie alle bekannten Teilchenwechselwirkungen des Standardmodells der Teilchenphysik und darüber hinaus simulieren können.. In der neuesten Version von Sherpa 3.0.0, einem hadronischen Eventgenerator, können die Polarisationszustände von intermediären Vektorbosonen simuliert werden. Der Eventgenerator MadGraph, ein Mehrzweck-Partonlevel-Eventgenerator, ist bereits in der Lage, diese Polarisationszustände zu simulieren, sodass die Ergebnisse beider Simulationsprogramme für die $W^{\pm}Z$-Produktion miteinander verglichen werden können. Eine weitere sinnvolle Möglichkeit, um zu überprüfen, ob Sherpa die Effekte der Vektorbosonpolarisation simulieren kann, ist es, theoretische Auffälligkeiten, wie der Radiation Amplitude Zero Effekt, wo der differentielle Wirkungsquerschnitt bei einer bestimmten Observable gleich Null ist, zu untersuchen.
In vielen Modellen, welche die Physik jenseits des Standardmodells diskutieren, sind die Kopplungsparameter leicht verändert, was sich auf Polarisationseffekte auswirkt. Wenn also die Simulationsergebnisse sich von den Erwartungen des Standardmodells unterscheiden, kann die Auswahl für das richtige dieser Modelle eingeschränkt werden.

Contents

List of Figures

List of Tables

Acronyms and Conventions

SM	Standard Model (of particle physics)
RAZ	Radiation amplitude zero
LO	Leading order
VB	Vector boson
EW	Electroweak
BSM	Beyond Standard Model physics
ESB	Electroweak symmetry breaking
CERN	European Organisation for Nuclear Research
LHC	Large Hadron Collider
HEP	High energy physics
PID	Particle ID
PDF	Parton distribution function

1 Introduction

The Standard Model (SM) is the fundamental theory of particle physics. The goal in particle physics is to see if the SM can withstand new experiments and if results of experiments can be proven and interpreted by a new theory, if they could not be explained so far. Until now, no anomaly have been found in the SM. At the same time, it is known that this theory is not complete because it can not explain the matter-antimatter-asymmetry, dark matter or gravitation. In between the observations and the theory are simulation programs, so-called event generators. Their primary task is to simulate expected values and behaviors of the SM. They also create an important connection between observations and theory, because they can help to better understand existing experimental setups or create new ones.

This thesis focuses on the research of the polarization effects in the production of $W^{\pm}$- and Z-bosons, which are the so-called gauge bosons of the weak interaction. These effects are investigated in proton-proton collisions similar to the experiments at the LHC and in quark-antiquark and lepton-neutrino collisions in the Monte Carlo event generator Sherpa [1]. The results include a comparison between Sherpa and another simulation program, MadGraph [2], at the LHC-like environment. Also, a comparison between Sherpa and theoretical values in the quark-antiquark and lepton-neutrino collisions is performed.

In the newest module of Sherpa [3], one is able to simulate the polarization effects of intermediate $W^{\pm}$-, Z-bosons and photons, which are vector bosons (VBs). It is important to find out if the simulated results are consistent with the data of MadGraph and the theoretical calculations. If these results are unambiguous, the new module is working for the $W^{\pm}$- and Z-bosons.

Measuring the polarization effects of VBs offers possibilities to find potential anomalies in the SM because many models covering physics beyond the SM (BSM) often assume modifications in the electroweak theory. In numerous BSM models, triple and quartic gauge coupling vertices, contributing to VB-production processes, have different values for the gauge coupling parameters. Because the Higgs mechanism explains the longitudinal polarization states of the massive VBs ($W^{\pm}$ and Z), these states are directly connected to the electroweak symmetry breaking (ESB). If the Higgs mechanism works differently as expected up to now, this should affect polarization effects.

2 Basic Foundations

In this chapter, all important theoretical information is given to understand the following chapters. It includes an overview over the Standard Model, which forms the core of particle physics, a brief introduction to the used event generator Sherpa and a summary of the particle process this thesis is investigating.

2.1 The Standard Model

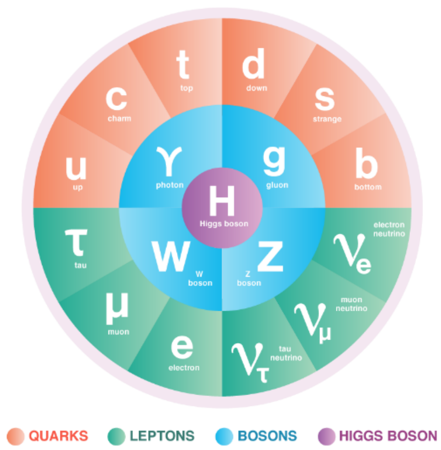

Figure 1: The particle content of the Standard Model of particle physics from Ref. [4].

The Standard Model of particle physics, as seen in figure (1), describes all elementary particles humanity has discovered so far. A particle is elementary if it does not have a measurable size and cannot be split into other particles, which should not be confused with the decay of some elementary particles.
The SM consists of twelve fermions, having a spin of $\frac{1}{2}$, four types of gauge bosons, having a spin of 1, and the Higgs boson, having a spin of 0. The fermions can be split into three generations: (e, ν_e, u, d), (μ, ν_μ, c, s) and (τ, ν_τ, t, b). The physical properties[1] of each fermion are shown in table 2.1. It describes three of the four fundamental interactions: the electromagnetic, the weak and the strong interaction. The fourth one, the gravitational interaction, is not yet described within the SM. This is partly because the gravitational interaction is weaker by many orders of magnitude at a microscopic level.

[1]In high energy physics (HEP), which includes particle physics, natural units are used [5].

The electromagnetic interaction, whose underlying theory is the "quantum electrodynamics" (QED), acts on every electromagnetically charged object. In particle physics, this interaction is described by the exchange of a photon γ between the two charged particles. How strong the interaction between two particles is depends on the charge of both particles. In group theory, the electromagnetic interaction can be described by the group U(1) [6].
The weak interaction acts on every particle which has a weak isospin I_3. The gauge bosons of the weak interaction are the W^+-, W^- and Z-boson. The $W^\pm$-bosons are electrically positive or negative and the Z-boson is neutral.
The helicity is the projection of the spin onto the momentum. For fermions, the helicity states can be either +1 or −1. In the SU(2)-group, how the weak interaction is described in group theory, the fermions differ in their chirality. A right-handed fermion has a helicity of +1 and a left-handed fermion has a helicity of −1. Both get treated differently by the SM. The left-handed fermions and right-handed antifermions are described by doublets in the SU(2)-group while the right-handed fermions and left-handed antifermions are described by singlets. Examples for left-handed doublets are $\begin{pmatrix} \nu_e \\ e^- \end{pmatrix}_L$ and $\begin{pmatrix} u \\ d \end{pmatrix}_L$. The doublets are similar for the other generations and similar for the right-handed antifermion doublets. In each doublet, the upper particle has a weak isospin of $I_3 = +\frac{1}{2}$ and the lower particle gets $I_3 = -\frac{1}{2}$ [6].
The strong interaction, whose underlying theory is the "quantum chromodynamics" (QCD), acts on every particle which has a "color" charge. The name color comes from the similarity of the charge to the RGB-color-system. The only particles which have a color charge are the quarks and gluons. The quarks can have the colors green, red or blue and the antiquarks can have the corresponding anticolors, e.g., antigreen. The gluons g are the gauge bosons of the strong interaction. They are electrically neutral, and each gluon carries a color and an anticolor. In total, described by the SU(3)-group which is the group of QCD in group theory, there are eight gluons, six gluons can change the color of a quark or gluon and two gluons do not change the color. By making every possible combination between the colors and anticolors, there are nine different gluons. Three of those combinations have superpositions of the same color-anticolor-combination and one of them is colorless, making it not able to interact via the QCD. Quarks can be combined to form colorless hadrons, most notably the baryons (qqq) and the mesons ($q\overline{q}$). The two earliest known baryons are the proton (uud) and neutron (udd). It is impossible to separate quarks from each other since the energy to separate the quarks from a bound state is linearly proportional to the distance between two quarks. Before two quarks would be separated, a new $q\overline{q}$-pair would have been formed [6].
Some extensions of the SM include the gravitational interaction which also has a hypothetical gauge boson, the graviton G with a spin of 2. It has not been discovered yet.
The Higgs-boson is an excitation of the Higgs-field which is present everywhere in the universe. The Higgs-boson can interact with every particle which has a mass [6]. The Higgs mechanism which introduces the Higgs-boson is described in more detail in section 2.1.1.

For every charged particle there is an antiparticle with opposite charge. The antiparticle can be labeled either with its charge or by writing $\overline{P}$ corresponding for the particle P.

Generation	1			2			3		
Particle	e	u	d	μ	c	s	τ	t	b
Charge [e]	-1	2/3	-1/3	-1	2/3	-1/3	-1	2/3	-1/3
Mass [MeV]	0.511	2.16	4.67	105.658	1270	93400	1776.860	172690	4180

Table 2.1: Physical properties of the elementary particles [7]. The neutrinos are not listed, all of them are electrically neutral and their mass can be approximated with zero.

2.1.1 Polarization of $W^{\pm}$- and Z-bosons

Like the photon and gluon, both the $W^{\pm}$- and the Z-boson have transversal polarization states, spin up and spin down. Unlike the photon and the gluon they are not massless, which results in an additional polarisation state called longitudinal.
In the 1960's, Glashow [8], Salam [9], and Weinberg [10] (GSW) unified the weak and the electromagnetic interaction to the electroweak theory. In group theory, the electroweak theory is described by the $SU(2)_L \times U(1)_Y$ gauge symmetry. When introducing the Higgs mechanism, this gauge symmetry is broken spontaneously by choosing a specific vacuum state for the Higgs-field without loss of generality. The $SU(2)_L \times U(1)_Y$-group has four degrees of freedom which the Higgs mechanism is not allowed to change. The four new degrees of freedom are the massive Higgs-boson and three massless Goldstone-bosons which prove to be not physical and can be eliminated by a specific gauge transformation. After applying a doublet of complex scalar fields, a detailed description of this process can be found in [11, 6], the three Goldstone-bosons turn out to be the longitudinal polarization states of the weak gauge-bosons [11].

2.2 The Simulation of Particle Collisions with Sherpa

The biggest particle accelerator in the world, the LHC (Large Hadron Collider) at the CERN (European Organization for Nuclear Research, the facility is named after the founder organization Conseil européen pour la recherche nucléaire) in Geneva, Switzerland, is capable of accelerating protons close to the speed of light.
Simulation programs are used as a transition from theory to experiment and from experiment to theory. The detectors at the LHC normally detect over one hundred particles from a single particle collision. These particles can have momenta over several orders of magnitude. Scientists have to identify all those particles from the broad range of particles included in the SM or even beyond the SM [12]. Some of the many benefits of event generators are given in Ref. [12], like to extract signals from background data, to compare their predictions with

data to perform measurements of SM parameters or providing realistic input to design new experiments.

The simulation program used for this thesis is the Sherpa (Simulation of High-Energy Reactions of PArticles) event generator [13, 14].

2.2.1 Particle Collision at the LHC

The LHC consists of a storage ring with a total circumference of about 27 km [15]. With the help of superconductive magnets, it is able to accelerate protons to an energy of about 6.8 TeV in the third and latest run. Since the LHC can accelerate two beams at once, the total usable energy in a collision, the center of mass energy $\sqrt{s}$, is 13.6 TeV. There are a total of four detectors built at the accelerator: ATLAS (used as proper name), CMS (Compact Muon Solenoid), ALICE (A Large Ion Collider Experiment) and LHCb (LHC beauty) [15]. All detectors are built at a point in the LHC where both beams collide.

2.2.2 The Sherpa Event Generator

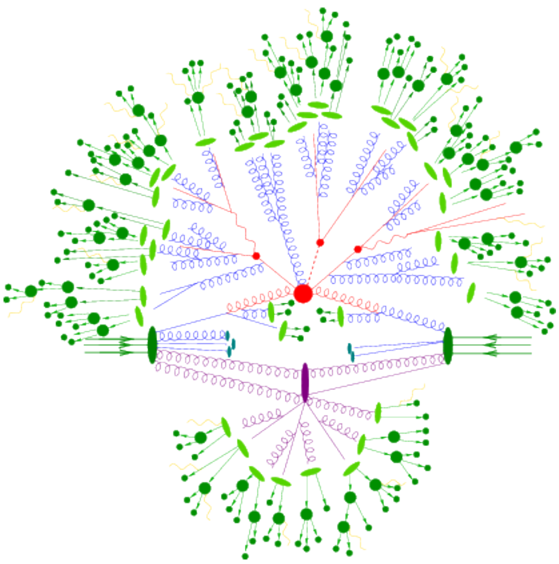

Figure 2: Visualization of a particle collision in Sherpa [16]. To the left and to the right are the incoming beams (green). Some partons interact in hard processes (red blobs), some interact in underlying processes (purple blob), and some are beam remnants which do not interact at all (light blue). The red and blue curly lines are parton showers. The light green blobs show the hadronization of partons. The dark green blobs and lines describe the decay of unstable hadrons. During a particle collision, every charged particle can emit a photon at any time which can lead to electromagnetic showers by electromagnetic pair production and annihilation.

In particle collision simulations, there are three energy regimes which must be treated separately. At high energy scales like at the LHC, the beam constituents, quarks or gluons which are called partons in this case, interact and produce a small number of highly energetic particles. This regime, also known as "hard processes", is perturbatively computable. At low energy

scales, at the order of 1 GeV, the incoming partons are confined and the outgoing partons form stable hadrons. These "soft processes" have to be modelled since the outgoing partons form the observed final-state hadrons by interacting non-perturbatively which cannot yet be calculated. The third regime is the energy region between the other regimes. Here, the calculations are dominated by perturbative effects from QCD, whose consequence is the formation of so-called "jets" which develop by quarks emitting gluons which can create quarks by pair production until they are at low energy scales to form stable hadrons. Since there are so many particles to compute and integrate over many phase-space dimensions, the simulation can be computed well with Monte Carlo techniques [12].
For the Sherpa event generator, one can set-up run-cards, as seen in appendix B, for a process. Then Sherpa can run a process many times in one command. How those run-cards are set-up and what settings are available to choose can be found in the Sherpa manual [17].

Monte Carlo Method

There are multiple Monte Carlo methods. In Sherpa, the Monte Carlo integration method is used.
When particles collide, a large number of different final states can be produced. To calculate the cross-section of a process, one needs to know all possible matrix elements squared $f(X)$. X contains all four-momenta of the interacting particles. Sherpa then needs to integrate over all four-momenta. Since the ranges of the four-momenta can differ in a wide range in particle collisions, using standard integration methods like Gaussian would be too slow or inaccurate. Therefore, the Monte Carlo integration method is especially useful for particle collisions.
In the easiest Monte Carlo integration method, the needed integral

$$I[f] = \int_V d^n x f(X)$$

can be approximated by the central limit theorem of statistics using N (pseudo-)randomly distributed points $X_i, i \in \{1 \dots N\}$ in the phase-space with

$$I[f] \simeq \langle f \rangle = \frac{1}{N} \sum_{i=1}^{N} f(X_i).$$

The error $E[f]$ is given by

$$E[f] = \sqrt{\frac{\mathrm{Var}(f)}{N-1}}$$

which shows that the Monte Carlo method gets more accurate, the more points are used.
A more efficient way to integrate using Monte Carlo integration is by using importance sampling. In Sherpa, a type of importance sampling is used. How importance sampling works is

described in Ref. [12].

2.3 The Process of Inclusive W$^{\pm}$Z-production

The W$^{\pm}$Z-production process can happen when two fermions, one normal particle and one antiparticle, collide. At the LHC the process happens with the quarks from the protons, but it can also happen in collisions using leptons and their neutrinos, although there is no neutrino accelerator. The general reaction in a proton accelerator is $p + p \Rightarrow W^{\pm} + Z$. The coupling order of this process is $\mathcal{O}(\alpha_{EW}^2)$. In this process it is interesting to see how the polarizations of the VBs impact the differential cross-section of this process.
The four-momenta participating in the W$^{\pm}$Z-production at LO are, when assuming that the incoming beam axis is parallel to the z-axis, $p_1 = E(1, \vec{e}_z)$, $p_2 = E(1, \vec{e}_z)$, $p_W = (E_W, \vec{p})$ and $p_Z = (E_Z, -\vec{p})$, where E is the beam energy of the incoming beams, $\vec{e}_z = (0, 0, 1)$ is the unit vector in the direction of the beam axis, E_W, E_Z are the kinetic energies of the W$^{\pm}$- and Z-bosons and $\vec{p} = p(\sin\theta\cos\varphi, \sin\theta\sin\varphi, \cos\theta)$ is the momentum of the W$^{\pm}$- and Z-bosons after the collisions.

The calculation of the sum of all matrix elements of the Feynman-diagrams in figure (3) is

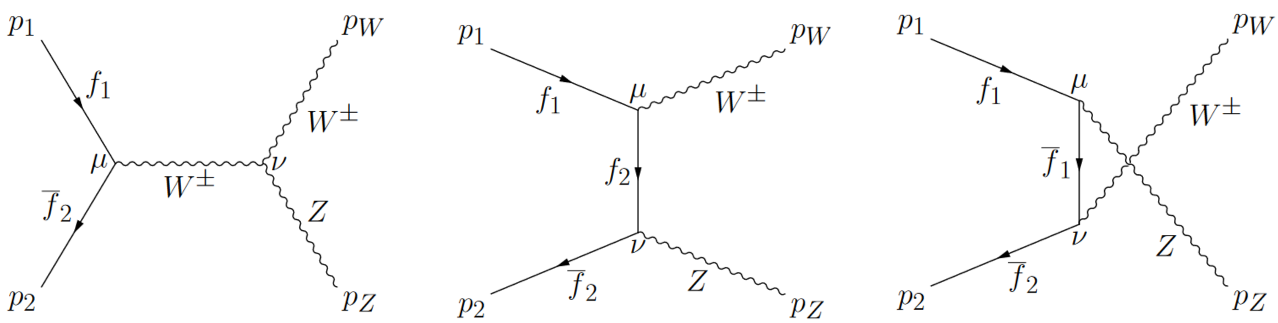

(a) s-channel **(b)** t-channel **(c)** u-channel

Figure 3: All possible Feynman-diagrams for the W$^{\pm}$Z production at LO

given in Ref. [18] by

$$\mathcal{M}(\lambda_W, \lambda_Z) = F\varepsilon^*_{\lambda_W \mu}(p_Z)\varepsilon^*_{\lambda_Z \nu}(p_Z)\overline{v}(p_2)T^{\mu\nu}\frac{1}{2}(1-\gamma^5)u(p_1) \tag{1}$$

with

$$T^{\mu\nu} = g_-^{f_1}\gamma^\mu \frac{\not{p}_1 - \not{p}_Z}{u}\gamma^\nu + g_-^{f_2}\gamma^\nu \frac{\not{p}_1 - \not{p}_W}{t}\gamma^\mu + \frac{Q_W \cot\theta_W}{s - m_W^2}[(\not{p}_Z - \not{p}_W)g^{\mu\nu} + 2p_W^\nu\gamma^\nu - 2p_Z^\mu\gamma^\nu], \tag{2}$$

where $\not{a} = \gamma^\sigma a_\sigma$ for any four-vector a_σ. The Dirac-matrices γ^σ are (4x4)-matrices and defined by

$$\gamma^0 = \begin{pmatrix} 1 & 0 \\ 0 & -1 \end{pmatrix}, \ \gamma^i = \begin{pmatrix} 0 & \sigma_i \\ -\sigma_i & 0 \end{pmatrix}, \ \gamma^5 = \begin{pmatrix} 0 & 1 \\ 1 & 0 \end{pmatrix},$$

where 1 is the (2x2)-identity, the σ_i are the Pauli-matrices and γ^5 can be calculated by $\gamma^5 = i\gamma^0\gamma^1\gamma^2\gamma^3$. $\overline{v}(p_2) = v(p_2)\gamma^0$ and $u(p_1)$ are the spinors of the fermions. $\varepsilon_\lambda(p)$ is the polarization-vector of a boson (in this case W$^{\pm}$ or Z). The polarizations can be transversal (shown either as $\pm$ or T) or longitudinal (shown either as 0 or L). F contains the factors each matrix-element has in common:

$$F = C\frac{e^2}{\sqrt{2}\sin\theta_W},$$

where $C = 1$ for leptons and $C = \delta_{c_1c_2}V_{f_1f_2}$ for quarks where c_i are the colors of the corresponding quark. θ_W is the weak mixing angle ($\cos\theta_w = \frac{m_W}{m_Z}$) where $m_W = 80.377$ GeV [7] is the mass of the W$^{\pm}$-boson and $m_Z = 91.1876$ GeV [7] is the mass of the Z-boson. $g_-^{f_i}$ are the couplings between the Z-boson and left-handed fermions:

$$g_-^{f_i} = \frac{I_3^{f_i} - Q_{f_i}\sin^2\theta_W}{\sin\theta_W\cos\theta_W}.$$

$I_3^{f_i}$ is the weak isospin and Q_{f_i} is the charge of the fermion. Since one f_i is an antifermion, it is important to know that one uses the weak isospin and the charge of the corresponding fermion. The kinematic variables s, t, u are defined by

$$s = (p_1 + p_2)^2, \ t = (p_1 - p_W)^2 = -\frac{s}{2}(\alpha - \beta\cos\theta), \ u = (p_1 - p_Z)^2 = -\frac{s}{2}(\alpha + \beta\cos\theta), \quad (3)$$

where $\alpha = 1 - r_W - r_Z = \frac{2}{s}(E_W E_Z + p^2)$, $\beta = (\alpha^2 - 4r_W r_Z)^{\frac{1}{2}} = \frac{2}{s}p(E_W + E_Z)$ and $r_V = \frac{m_V}{s}$ with $V = W, Z$. Using $g_-^{f_1} - g_-^{f_2} = Q_W\cot\theta_W$ and $s + t + u = m_W^2 + m_Z^2$, Eq. (1) can be rewritten as

$$\mathcal{M}(\lambda_W, \lambda_Z) = \frac{F}{s}\overline{v}(p_2)\left[X\left(\not{A} - \frac{t}{s - m_W^2}\not{V}\right) + Y\not{V}\right](1 - \gamma^5)u(p_1). \quad (4)$$

Here, X and Y are combinations of the couplings and $\not{A}$ and $\not{V}$ contain the polarization dependent parts:

$$X = \frac{s}{2}\left(\frac{g_-^{f_1}}{u} + \frac{g_-^{f_2}}{t}\right), \ Y = g_-^{f_1}\frac{s\,m_Z^2}{2u(s - m_W^2)} \quad (5)$$

$$\not{A} = 2p_1 \cdot \varepsilon_W^* \not{\varepsilon}_Z^* + \not{\varepsilon}_Z^* \not{\varepsilon}_W^* \not{p}_W, \; \not{V}, = 2[\varepsilon_W^* \cdot \varepsilon_Z^* \not{p}_Z + p_Z \cdot \varepsilon_Z^* \not{\varepsilon}_W^* - p_Z \cdot \varepsilon_W^* \not{\varepsilon}_Z^*]. \tag{6}$$

Now, one can insert the different polarizations of the W$^{\pm}$- and Z-boson, $\lambda_W, \lambda_Z \in \{\pm, 0\}$. The resulting matrix-elements $\mathcal{M}(\lambda_W, \lambda_Z)$ [18] are:

$$\mathcal{M}(\pm, \mp) = F \sin\theta(\lambda_W - \cos\theta)X, \tag{7}$$

$$\mathcal{M}(\pm, \pm) = F \sin\theta \left[\left(\lambda_W(r_Z - r_W) - \beta + \cos\theta + \beta \frac{\alpha - \beta\cos\theta}{1 - r_W} \right) X + 2\beta Y \right], \tag{8}$$

$$\mathcal{M}(0, 0) = F \frac{\sin\theta}{\sqrt{4 r_W r_Z}} \left[\left(-\beta\rho + \beta_W \beta_Z \cos\theta + \beta\rho \frac{\alpha - \beta\cos\theta}{1 - r_W} \right) X + 2\beta\rho Y \right], \tag{9}$$

$$\mathcal{M}(\pm, 0) = F \frac{1 - \lambda_W \cos\theta}{\sqrt{2 r_Z}} \left[\left(2\lambda_W r_Z - \beta + \beta_Z \cos\theta + \beta \frac{\alpha - \beta\cos\theta}{1 - r_W} \right) X + 2\beta Y \right], \tag{10}$$

$$\mathcal{M}(0, \pm) = F \frac{1 + \lambda_Z \cos\theta}{\sqrt{2 r_W}} \left[\left(-2\lambda_Z r_W - \beta + \beta_W \cos\theta + \beta \frac{\alpha - \beta\cos\theta}{1 - r_W} \right) X + 2\beta Y \right]. \tag{11}$$

Here $\beta_W = 1 + r_W - r_Z$, $\beta_Z = 1 - r_W + r_Z$ and $\rho = 1 + r_W + r_Z$.
The radiation amplitude zero (RAZ) effect describes a cross-section being equal to zero for a certain region of the phase-space. Since the cross-section is proportional to $\mathcal{M}^2$, this only happens if the matrix-element is zero. Although all possible polarization combinations can be zero at $\theta \in \{0, \pi\}$, those angles cannot be measured by the structure of the detectors since at those angles, the focused particle-beams fly into the detector. Therefore, the RAZ effect only occurs in $\mathcal{M}(\pm, \mp)$, when $X = 0$.
To detect W$^{\pm}$- and Z-bosons, one has to detect their decay products. The W$^{\pm}$-boson can decay via $W^{\pm} \to l^{\pm} + \overset{(-)}{\nu_l}$ or $W^{\pm} \to q_i + \overline{q}_j$. The Z-boson can decay via $Z \to q + \overline{q}$, $Z \to l^+ + l^-$ and $Z \to \nu_l + \overline{\nu}_l$. Here, l can be any lepton and q is any quark besides the top-quark. In this thesis, only the decays to the leptons are of interest, excluding the tauons τ since they decay very quickly. Nevertheless, there are analyses able to handle the hadronic decays [19].

3 Phenomenological Study of the Radiation Amplitude Zero Effect in $W^{\pm}Z$-production

In this chapter, the results of the study of the radiation amplitude zero effect in $W^{\pm}Z$-production with Sherpa are illustrated. First the results of the RAZ in proton-proton collisions with Sherpa are presented and compared to MadGraph, another event generator capable of generating events with polarized $W^{\pm}$- and Z-bosons. After that, the RAZ is investigated in fixed-parton collisions which is then contrasted to analytical calculations. While protons consist of many partons, fixed-parton means that one is only interested in the parton itself. The $W^{\pm}Z$-production works with fermions, as seen in section 2.3, which means both quarks and leptons can be used to produce $W^{\pm}Z$. After the fixed-parton investigation, the RAZ is studied in electron-neutrino collisions and again compared to analytical calculations.
The most interesting observable connected to the final state for these examinations is the polar scattering angle relative to the beam axis θ. In the histograms from Sherpa, the differential cross-section in dependency of the measured observable of interest is displayed on the y-axis, and in the histograms from MadGraph [20], the number of events is displayed on the y-axis. Although both quantities are different, the differential cross-section and the number of events are proportional to each other, so it is valid to compare them each other.

3.1 RAZ in Proton-Proton Collisions

In this section, collisions between two protons are studied. This setup is meant to simulate the physics happening in proton-proton accelerators. The results are shown for the productions of $W^{\pm}Z$ + 0 jets ($\mathcal{O}(\alpha_{EW}^2)$), $W^{\pm}Z$ + 1 jet ($\mathcal{O}(\alpha_s\alpha_{EW}^2)$) and $W^{\pm}Z$ + 0+1 jets.

3.1.1 Results from Sherpa

For proton-proton collisions, the $W^{\pm}Z$-productions is simulated in three different setups: $W^{\pm}Z$ + 0 jets, called 0J in this thesis, $W^{\pm}Z$ + 1 jet, called 1J and $W^{\pm}Z$ + 0+1 jets, called 0+1J.
In Sherpa [21, 3], the different polarizations of $W^{\pm}$- and Z-bosons are all simulated during a

single run without needing to specify which polarization one wants to simulate. To differentiate between the different polarizations, Sherpa assigns each polarization a weight with associated name.

Simulation Setups

The analysis used to obtain the data from the simulated events was originally created by Prachi Arvind Atmasiddha [22] whose results from MadGraph [23] will be compared with the results from Sherpa. This analysis is a Rivet [24] analysis where several types of histograms can be created and filled with observables calculated from the data. In this analysis, the histograms are filled with the differential cross-section as depending on the observables. To fit the analysis to the needed results, histograms where only $\cos\theta$ of the W^-- and W^+-boson are the observables are added. For each of the W^-- and W^+-boson, one run-card is used which can be seen in appendix B and with both run-cards, the same number of events are generated. The analysis only uses events whose final state consists of three leptons and one neutrino (not including τ and ν_τ). For these studies, the only studied decays of the $W^{\pm}$- and Z-bosons are those that result in electrons and muons in the final state. These decays can be forced in Sherpa as viewable in appendix B.
For all three setups the physical properties are noted in table 3.1. The merging scale is called "CKKW" and defines which minimum energy an additional jet has to have to be calculated in the hard matrix element. The core scale is needed for factorization and renormalization [11] calculations. The widths of $W^{\pm}$ are set to zero because Sherpa applies the Narrow Width Approximation [25]. Otherwise, this approximation would not be consistent and the so-called "Ward identities" [26] would be violated. To identify particles, each has a corresponding particle ID (PID) [27] which are used in Sherpa. To describe how the partons are distributed in the proton, parton distribution functions (PDF) are used. In Sherpa, one can set different PDF sets which contain multiple PDFs. The PDF set used in these simulations is "NNPDF30_nlo_as_0118".
The differences between the run-cards for each setup is given in appendix B.

Results from the 0J Setup

In figure (4), the histograms of the $W^{\pm}$-boson polar scattering angle in the center of mass frame of the diboson pair ($W^{\pm}$- and Z-boson) are displayed. There is one histogram for each selection criteria (coll.: cuts) described in table 3.2. The first criterion does not have any selection criteria, it does not remove any events. The second criterion, the lepton cuts, removes every event in which the leptons from the $W^{\pm}$- and Z-boson decays do not fit the criteria given in table 3.2. The third criterion, the $p_{T,WZ}$ cut, removes every event in which the total transverse

Setup	0J	1J	0+1J
Process	$p+p \to W^{\pm}+Z$	$p+p \to W^{\pm}+Z+j$	$p+p \to W^{\pm}+Z+(j)$
Decays	$W^{\pm} \to l^{\pm} + \overset{(-)}{\nu_l},\ Z \to l^{+}+l^{-}$		
Coupling order	$\mathcal{O}(\alpha_{EW}^4)$	$\mathcal{O}(\alpha_s \alpha_{EW}^4)$	$\mathcal{O}((1+\alpha_s)\alpha_{EW}^4$
Merging scale [GeV]	not used	not used	20
Core scale	$0.25\,\lvert p_W + p_Z\rvert^2$		
Changed widths	$\Gamma_W = 0,\ \Gamma_Z = 0$		
Beams	2 proton beams (each $E = 6500$ GeV)		
Center of mass energy $\sqrt{s}$ [TeV]	13		

Table 3.1: Physical properties of the used setups. The coupling order includes the decays.

momentum of the $W^{\pm}$- and Z-boson does not fit and the fourth criterion, the $p_{T,Z}$ cut, removes every event in which the transverse momentum of the Z-boson does not fit. The black curve shows the total differential cross-section of all polarization states without interference, which appears when working with polarization of bosons. However, it is small enough, $\lesssim 1\%$, to be neglected in the following plots and tables. The orange, red, green, and blue curves show the differential cross-section of their respective polarization states TT, LT, TL, LL. The first letter indicates the polarization of the $W^{\pm}$-boson and the second letter indicates the polarization of the Z-boson. When $\cos\theta \approx 0$, the differential cross-section of TT is in its minimum which indicates that the RAZ appears there. Although the differential cross-section for LL is even lower at $\cos\theta \approx \pm 0.7$, the RAZ does not appear there since the total differential cross-section is dominated by the non-zero differential cross-section of TT.

Between figures (4a), (4b) and (4c) are only slight differences in the height of the curves,

Selection criterion	Settings
all events	no selection criteria
lepton cuts	$p_{T,l_W} > 20\,\mathrm{GeV}$, $p_{T,l_Z} > 15\,\mathrm{GeV}$ $\lvert\eta_l\rvert < 2.5$ $\lvert m_{ll} - m_Z\rvert < 10\,\mathrm{GeV}$ $m_T^W > 30\,\mathrm{GeV}$ $\Delta R(l_Z^+, l_Z^-) > 0.2$, $\Delta R(l_Z, l_W) > 0.3$
$p_{T,WZ}$ cut	$p_{T,WZ} < 70\,\mathrm{GeV}$
$p_{T,Z}$ cut	$p_{T,Z} > 200\,\mathrm{GeV}$

Table 3.2: All used selection criteria with the corresponding settings. p_T is the momentum perpendicular to the beam axis. $\eta = -\ln\tan\frac{\theta}{2}$ is the pseudorapidity which is approximately equal to the rapidity y in the ultrarelativistic limit. $m_T = \sqrt{E^2 - p_z^2}$ is the transverse mass. $\Delta R = \sqrt{(\Delta\eta)^2 + (\Delta\varphi)^2}$ is the distance between two particles in the η-φ-plane where φ is the azimuthal angle.

the order of magnitude of the differential cross-section and the uncertainties of the differential cross-section. The uncertainty differences are explained by the different amount of events which were used to fill the histograms. The general form of the curves stays the same. In

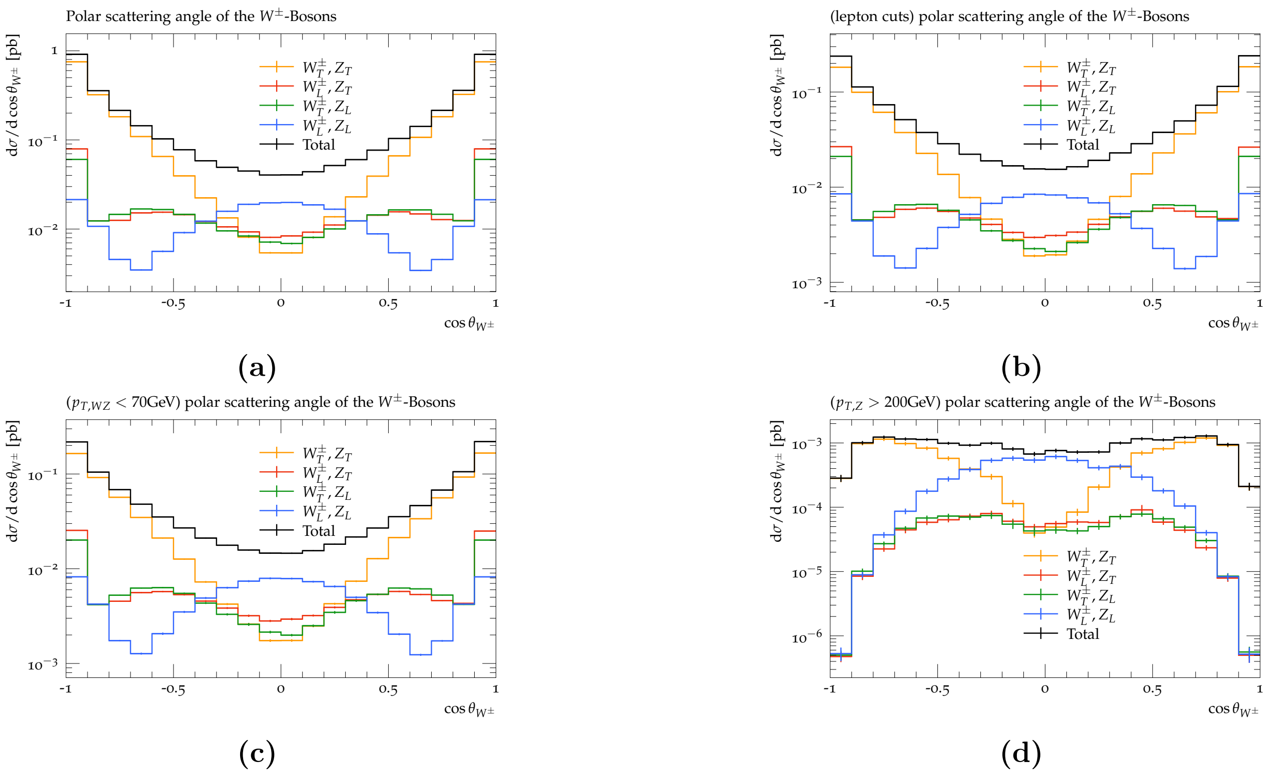

Figure 4: Histograms for the distributions of $\cos\theta$ of the $W^{\pm}$-boson with the 0J setup in the $W^{\pm}Z$-production process at $\sqrt{s} = 13$ TeV for (a) no selection requirements; (b) events after all lepton cuts; (c) events after the $p_{T,WZ}$ cut and (d) events after the $p_{T,Z}$ cut.

figure (4d), the form of the curves is different, but the RAZ is still visible.

Results from the 1J and 0+1J Setups

Figures (5) and (6) show the same observables with the same selection criteria for the other two setups. The major difference to the 0J setup is that the RAZ does not occur anymore, because although the differential cross-section of TT is in its minimum, it dominates the total differential cross-section, so it does not reach zero.

Between figures (5a) to (5d) are no other main differences compared to figure (4). The only difference between figures (5a) and (5c) is that the differential cross-section of LL is dominating for $\cos\theta \approx 0$ in figure (5c), which does not imply the RAZ since the differential cross-section of TT is not the lowest differential cross-section.

The results for the 0+1J setup in figure (6) are similar to the results for the 1J setup. The most noticeable difference is that the uncertainties in the 0+1J setup are larger than in the 1J setup.

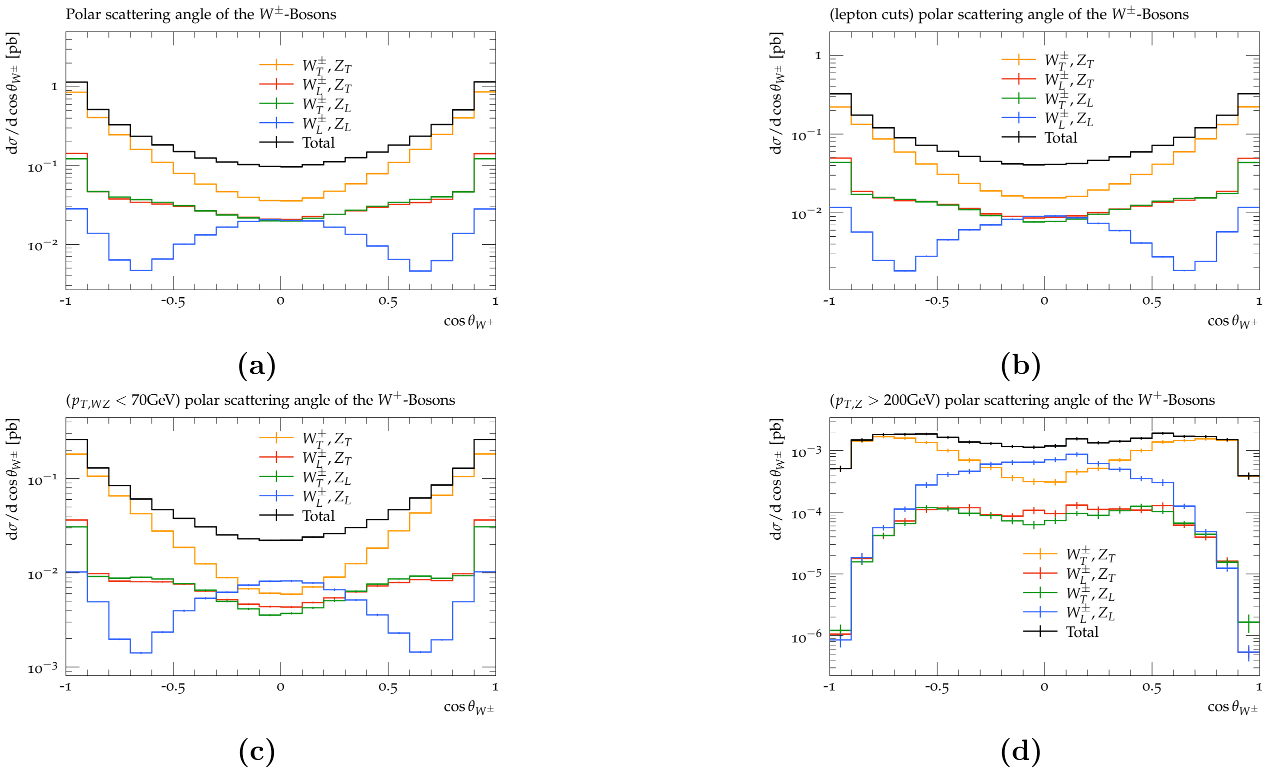

Figure 5: Histograms for the distributions of $\cos\theta$ of the $W^{\pm}$-boson with the 1J setup in the $W^{\pm}Z$-production process at $\sqrt{s} = 13$ TeV for (a) no selection requirements; (b) events after all lepton cuts; (c) events after the $p_{T,WZ}$ cut and (d) events after the $p_{T,Z}$ cut.

3.1.2 Comparison with Results from MadGraph

In this section, the results from Sherpa from the previous section are compared to another event generator: MadGraph. All MadGraph histograms are from Ref. [23]. In both results, the colors represent the same measured polarization states. Orange represents TT, red LT, green TL, blue LL and black depicts the sum of all polarization states.
Figure (7) illustrates the comparison of the polar scattering angle of the $W^{\pm}$-boson with the 0J setup and after the lepton cuts between Sherpa in figure (7a) and MadGraph in figure (7b). Both histograms look similar if one views the general steps between each bin and the relative distances between the curves. The RAZ is clearly visible, and it is also noticeable whether the LT- or TL-events contribute more to the differential cross-section. Around $\cos\theta = 0$ and at $\cos\theta = 1$, TL-events contribute more while in between, LT-events account for more to the differential cross-section.

In figures (8) and (9) one can see that the simulations in Sherpa and in MadGraph are similar as well. The only difference shows up in the simulations with the 1J setup where the differential cross-section in Sherpa, figure (9a), for LL is much closer and partially higher than the differential cross-section for TL and LT in comparison to the simulation in MadGraph, figure (9b).

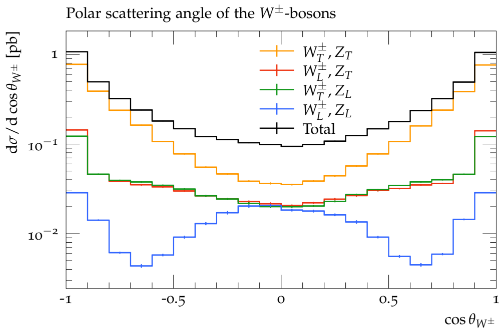

(a)

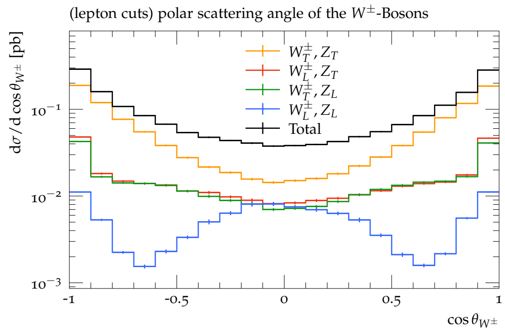

(b)

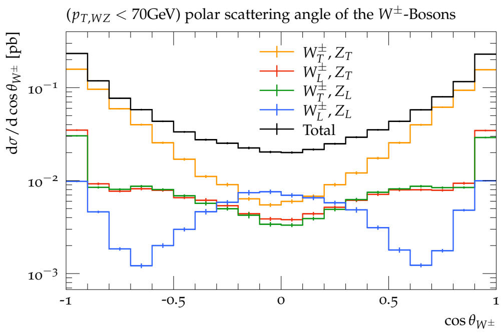

(c)

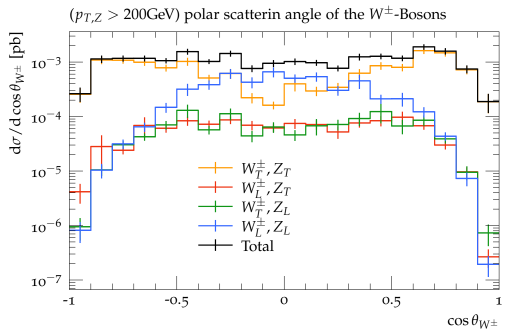

(d)

Figure 6: Histograms for the distributions of $\cos\theta$ of the W$^{\pm}$-boson with the 0+1J setup in the $W^{\pm}Z$-production process at $\sqrt{s} = 13$ TeV for (a) no selection requirements; (b) events after all lepton cuts; (c) events after the $p_{T,WZ}$ cut and (d) events after the $p_{T,Z}$ cut.

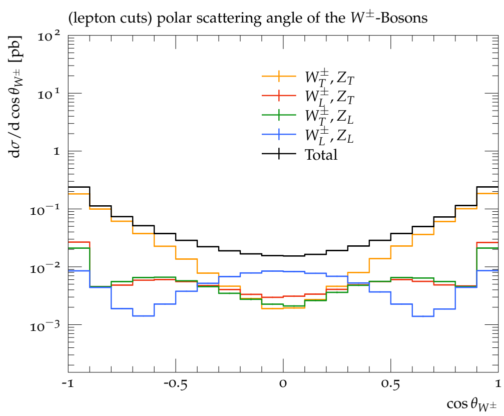

(a)

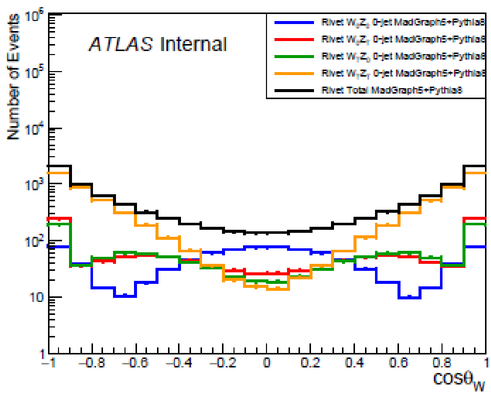

(b)

Figure 7: Comparison of $\cos\theta$ of the polarized distributions of the W$^{\pm}$-boson with the 0J setup in the $W^{\pm}Z$-production process and all events after the lepton cuts between Sherpa (a) and MadGraph from Ref. [23] (b).

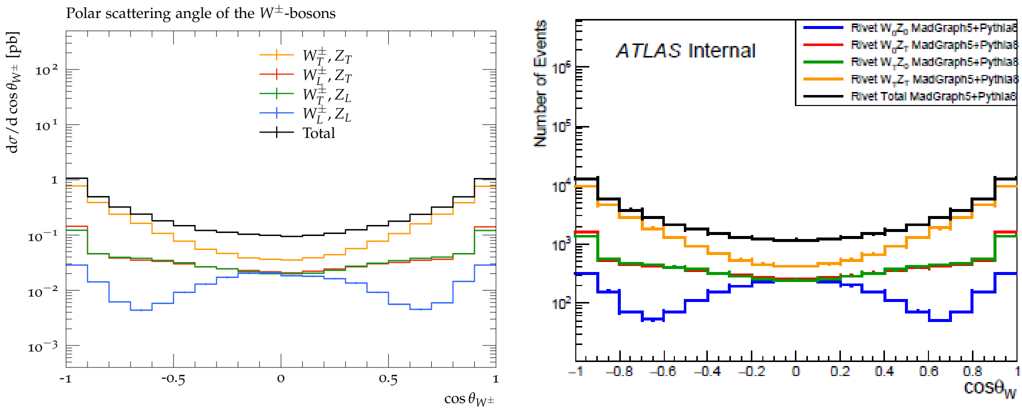

(a) (b)

Figure 8: Comparison of $\cos\theta$ of the polarized distributions of the $W^{\pm}$-boson with the 0+1J setup in the $W^{\pm}Z$-production process and all events between Sherpa (a) and MadGraph from Ref. [23] (b).

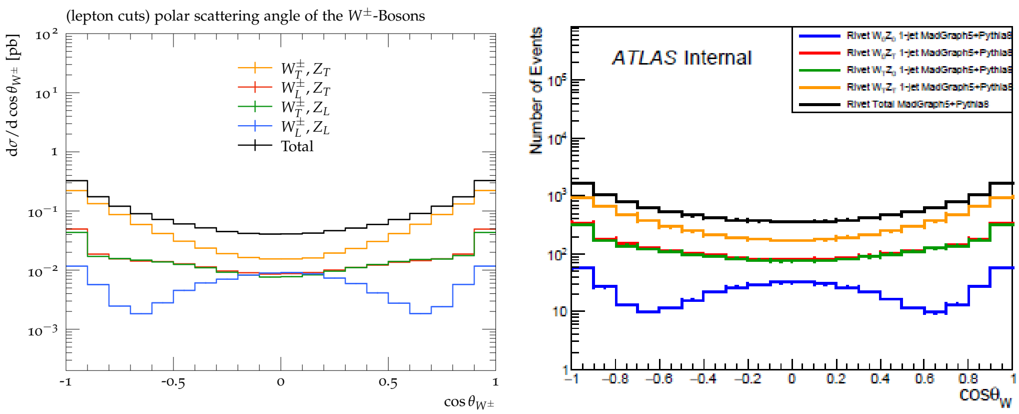

(a) (b)

Figure 9: Comparison of $\cos\theta$ of the polarized distributions of the $W^{\pm}$-boson with the 1J setup in the $W^{\pm}Z$-production process and all events after the lepton cuts between Sherpa (a) and MadGraph from Ref. [23] (b).

3.2 RAZ in Fixed-Parton Collisions

This section investigates the ability of Sherpa to simulate particle collisions where only partons are used as beams instead of hadrons. The goal is to see if Sherpa is able to simulate the RAZ effect for fixed-parton collisions.

3.2.1 Results from Sherpa

Fixed-parton collisions are generally possible to simulate with Sherpa by changing the corresponding beam PIDs and energies as seen in appendix B. To generate events which only depend on the hard process and the decays, one has to deactivate any option which simulates hadronization, parton or electromagnetic showering, including QED corrections or beam remnants. The corresponding run-cards with the different options can be seen in appendix B. For the fixed-parton collisions and later the lepton-neutrino collisions are only simulated without jets.

As explained in section 2.3 the RAZ effect only occurs in the TT-polarization, more specifically in the $\pm\mp$-polarization, and from section 3.1 only for LO, so the simulation is only done for LO, similar to the 0J setup from proton-proton collisions. In principle, it is possible to simulate the fixed-parton collisions for setups with more jets, but the expected difference would be the disappearance of the RAZ effect. To find out if and how the distributions change after modifying the energy, the events are generated with four different center of mass energies $\sqrt{s} \in \{400\ \text{GeV}, 2\ \text{TeV}, 13\ \text{TeV}, 200\ \text{TeV}\}$ of the parton-parton system. In comparison to the proton-proton collisions, the center of mass energy in fixed-parton collisions is higher because in a proton-proton system, the beam energies are distributed to all partons via the PDFs.

In figure (10), one sees the distributions for the W$^\pm$Z-production at fixed-parton level for the

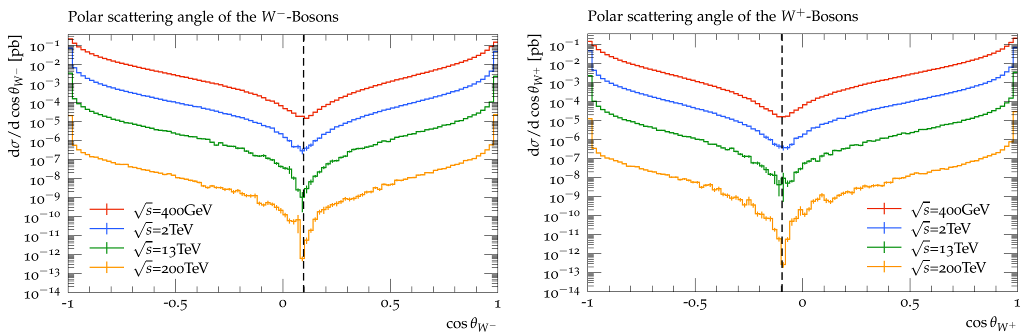

(a) $d + \overline{u} \rightarrow W^- + Z$ (b) $u + \overline{d} \rightarrow W^+ + Z$

Figure 10: Histograms for the distribution of $\cos\theta$ of the W$^-$- (a) and W$^+$-bosons (b) in the $W^\pm Z$-production process in fixed-parton collisions for the polarization combination TT at four different energies. The black dashed line marks the RAZ.

different energies. The most visible difference between the different values for $\sqrt{s}$ is that the differential cross-section drops with increasing energy. The RAZ can be seen for every energy but gets clearer the higher the energy is. The theoretical zero, called $\cos\theta_0$ in this thesis, can be identified at the inverse sign of the $W^{\pm}$-boson with the same absolute value: for the W^--bosons, $\cos\theta_0$ is within $[0.08, 0.10]$ and for the W^+-bosons, $\cos\theta_0$ is within $[-0.10, -0.08]$. More precise intervals can be achieved by changing the amount of bins in the code of the analysis. However, to achieve a similar low uncertainty, more events would have to be simulated. Why the zeroes differ depending on the sign of the $W^{\pm}$-boson is explained in section 3.2.2.

Table 3.3 shows the total cross-sections of the different polarizations at different energies calculated by Sherpa. Noticeable differences between the energies are the increasing domination of the TT polarizations and the decreasing values of the cross-sections with increasing energy. Table 3.3 only depicts the cross-sections for the W^-Z-production and combined transversal and longitudinal polarization states. More data with similar results can be found in appendix D in table D.2 for the W^+Z-production and combined transversal and longitudinal polarization states, in table D.1 for the W^-Z-production and all polarization states and in table D.3 for the W^+Z-production and all polarization states. The tables with all polarization states show that the fractions in the $\pm\mp$ polarizations are switched when the charge of the W-boson is changed.

Polarization	$\sigma/\sigma_{total}[\%]$
Total	100
W_0^-, Z_0	3.238
W_T^-, Z_0	3.610
W_0^-, Z_T	4.073
W_T^-, Z_T	89.122

(a) $\sqrt{s}$ = 400 GeV

Polarization	$\sigma/\sigma_{total}[\%]$
Total	100
W_0^-, Z_0	1.118
W_T^-, Z_0	0.076
W_0^-, Z_T	0.086
W_T^-, Z_T	98.718

(b) $\sqrt{s}$ = 2 TeV

Polarization	$\sigma/\sigma_{total}[\%]$
Total	100
W_0^-, Z_0	0.628
W_T^-, Z_0	0.001
W_0^-, Z_T	0.001
W_T^-, Z_T	99.367

(c) $\sqrt{s}$ = 13 TeV

Polarization	$\sigma/\sigma_{total}[\%]$
Total	100
W_0^-, Z_0	0.443
W_T^-, Z_0	0.000
W_0^-, Z_T	0.000
W_T^-, Z_T	99.554

(d) $\sqrt{s}$ = 200 TeV

Table 3.3: Fractions of the cross-sections for the W^-Z-production in fixed-parton collisions of the combined polarization states TT, TL, LT, LL for different center of mass energies.

3.2.2 Comparison with Analytical Calculation

From section 2.3 it is known that the RAZ effect only occurs for $\mathcal{M}(\pm,\mp)$ when setting X in Eq. 5 equal to zero. Since $\cos\theta$ is in u and t as it is visible in Eq. 3, one can rearrange the equation $X = 0$ to

$$\cos\theta_0 = \frac{\alpha}{\beta}\frac{g_-^{f_1} + g_-^{f_2}}{g_-^{f_1} - g_-^{f_2}} = -\frac{\alpha}{\beta}(Q_{f_1} + Q_{f_2})Q_W \tan^2\theta_w. \tag{12}$$

Because

$$\frac{\alpha}{\beta} = \frac{\sqrt{(m_W^2 + p^2)(m_Z^2 + p^2)} + p^2}{p(\sqrt{m_W^2 + p^2} + \sqrt{m_Z^2 + p^2})} \approx 1 \tag{13}$$

for $= p \geq 180$ GeV as seen in figure (C.1), Eq. 12 can be rewritten as

$$\cos\theta_0 = -(Q_{f_1} + Q_{f_2})Q_W \tan^2\theta_w. \tag{14}$$

Plugging in $(f_1,\ f_2) = (u,\ d)$ for the process $u + \overline{d} \to W^+ + Z$, gives $\cos\theta_0 = -\frac{1}{3}\tan^2\theta_w \approx -0.0957$ and vice versa $(f_1,\ f_2) = (d,\ u)$ for $d + \overline{u} \to W^- + Z$, gives $\cos\theta_0 = \frac{1}{3}\tan^2\theta_w \approx 0.0957$.

Both values are marked with a black dashed vertical line in figure (10) for the corresponding charge of the $W^{\pm}$-boson. It is clear to see that the simulation results agree with the theoretical value for the RAZ effect. Especially for $\sqrt{s} \in \{2\text{ TeV}, 13\text{ TeV}, 200\text{ TeV}\}$, the values coincide since $p > 180$ GeV is definitely given for all three energies. For $\sqrt{s} = 400$ GeV, the minimum is not so clear as for the other three energies and $|\cos\theta_0|$ might be a bit larger but still in the same bin of the histogram so it is not noticeable because p is in the same order of magnitude of 180 GeV, so $\frac{\alpha}{\beta} > 1$.

As described in [18], the RAZ effect in the TT polarization is determined by $\mathcal{M}(\pm, \mp)$ and not by $\mathcal{M}(\pm, \pm)$. This also can be seen in Sherpa when only looking at the polarizations $\pm\mp$ in figure (11a) and (11c) and $\pm\pm$ in figure (11b) and (11d). In the $\pm\mp$ graphs, the RAZ effect is clearly visible and in the $\pm\pm$ graphs it is not. By comparing both differential cross-sections, one can see that the differential cross-sections of the $\pm\mp$ polarizations are more dominant the higher the center of mass energy is. For a closer comparison between both polarization states, appendix C includes the graphs for each energy: $\sqrt{s} = 400$ GeV in figure (C.4), $\sqrt{s} = 2$ TeV in figure (C.6), $\sqrt{s} = 13$ TeV in figure (C.8) and $\sqrt{s} = 200$ TeV in figure (C.10).

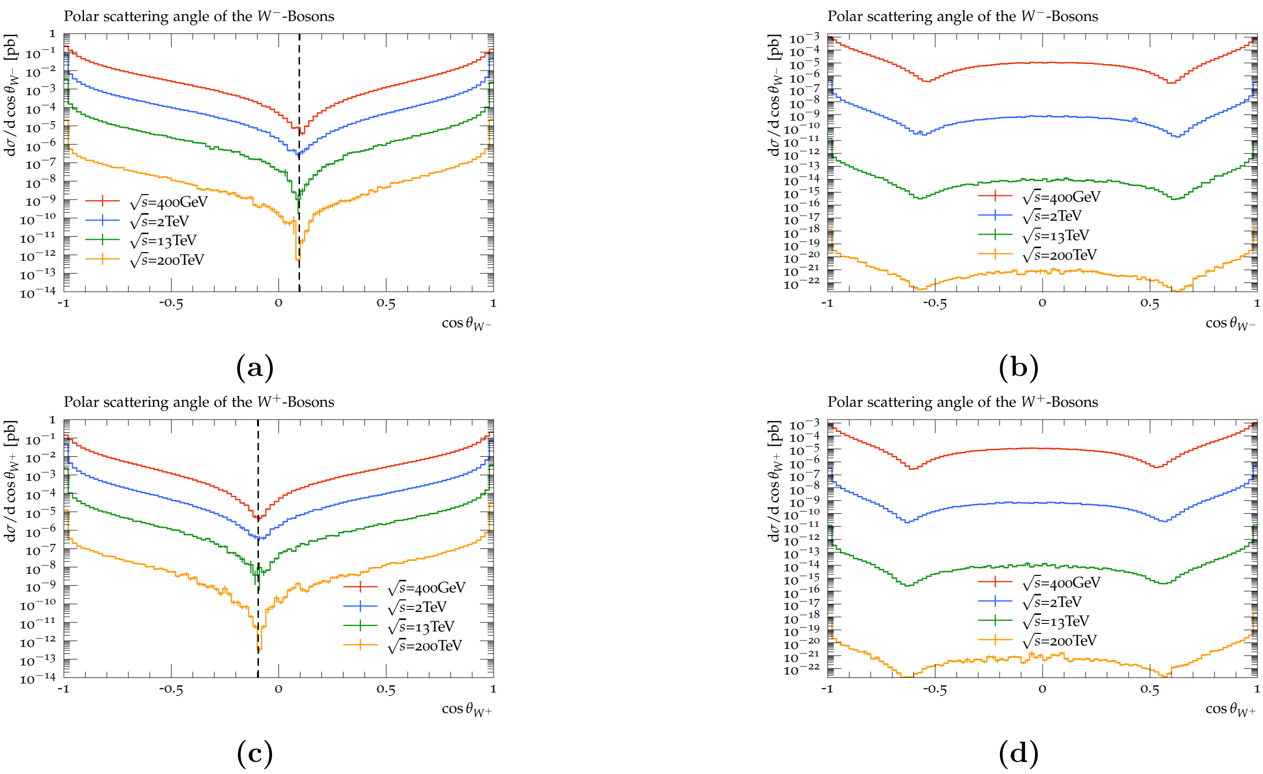

Figure 11: Histograms of the distribution of $\cos\theta$ of the W$^-$- (a, b) and the W$^+$-bosons (c, d) in the W$^\pm$-system in fixed-parton collisions for the polarization combinations $\pm\mp$ (a, c) and $\pm\pm$ (b, d) at four different energies. The black dashed line marks the RAZ.

3.3 RAZ in Lepton-Neutrino Collisions

This section investigates the simulation of RAZ in lepton-neutrino collisions, in particular $e^\pm \overset{(-)}{\nu}_e$ collision. Since there is no neutrino accelerator so far, the only way to get results for neutrino collisions is by simulating them.

3.3.1 Results from Sherpa

Sherpa is also able to simulate collisions between leptons. Similar to section 3.3.1, to simulate the process without any perturbations, the options to simulate hadronization, parton and electromagnetic showers are also turned off. For the subsequent studies, the corresponding run-cards can be found in appendix B.

In figure (12), the distributions for the W$^\pm$Z-production in lepton-neutrino collisions can be seen for a beam energy of $E = 13$ TeV. As in the fixed-parton collisions, the theoretical zeroes of the RAZ are at values of $\cos\theta$ with the same absolute value and opposite sign. For the W$^-$-bosons $\cos\theta_0$ is within $[-0.30, -0.28]$ and for the W$^+$-bosons $\cos\theta_0$ is within $[0.28, 0.30]$. Why the zeroes differ depending on the sign of the W$^\pm$-boson is explained in section 3.3.2

As readable in table B.4 with the translated PIDs, to simulate $\nu_e + e^+ \to W^+ + Z$ in Sherpa, the beams have to be defined in the order $[\nu_e,\ e^+]$. But the only viable way to simulate this

process is by defining the beams in the order [e^+, ν_e]. In Sherpa this order defines from which direction the particle is coming in. Since the polar scattering angle is defined by the beam axis of the incoming particle, the scattering angle of the W$^+$-bosons has the opposite sign. That is why the analysis is changed so every the polar scattering angle of every event which results in a W$^+$-boson has its sign flipped.
As seen in figures (12a) and (12b), the $\cos\theta$-distribution for both W$^{\pm}$Z-productions are as expected.

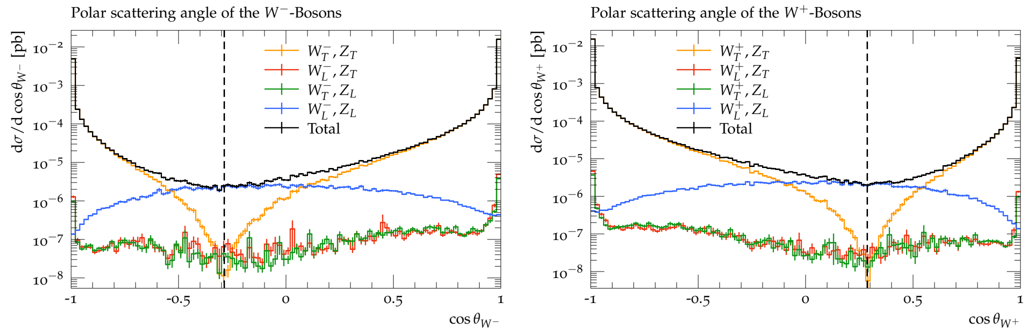

(a) $e^- + \overline{\nu_e} \to W^- + Z$ (b) $\nu_e + e^+ \to W^+ + Z$

Figure 12: Histograms for the distribution of $\cos\theta$ of the W$^-$- (a) and the W$^+$-bosons (b) in the $W^{\pm}Z$-production process lepton-neutrino collisions for the polarization combinations TT, TL, LT, LL at $\sqrt{s}$ = 13 TeV. The black dashed line marks the RAZ.

3.3.2 Comparison with Analytical Calculation

For both the W$^-$- and W$^+$-boson, the factor $(Q_{f_1} + Q_{f_2}) = -1$ needs to be included because only the charge of an electron is relevant for it. Thus, for $e^- + \overline{\nu_e} \to W^- + Z$, the RAZ is at $\cos\theta_0 = -\tan^2\theta_w \approx -0.2871$ and for $\nu_e + e^+ \to W^+ + Z$, at $\cos\theta_0 = \tan^2\theta_w \approx 0.2871$. Both values are approved by the simulations in figure (12).
As for the fixed-parton collisions, the domination of the RAZ effect by $\mathcal{M}(\pm,\mp)$ instead of $\mathcal{M}(\pm,\pm)$ can also be seen in Sherpa. It is observable in figure (13) that $\mathcal{M}(\pm,\mp)$ is dominating the differential cross-section of TT and is the only polarization combination to show the RAZ effect at the marked scattering angle. The differential cross-section of $\pm\pm$ is lower than the differential cross-section of $\pm\mp$ by a factor of about 10^{-4} and hence does not contribute much to the differential cross-section of TT. This can be confirmed by comparing the figures (12) and (13). Another way to show that $\mathcal{M}(\pm,\mp)$ is dominating the differential cross-section, is by looking at tables 3.4c and 3.4d. They show that the fractions of the $\pm\mp$ polarizations are by far the largest.

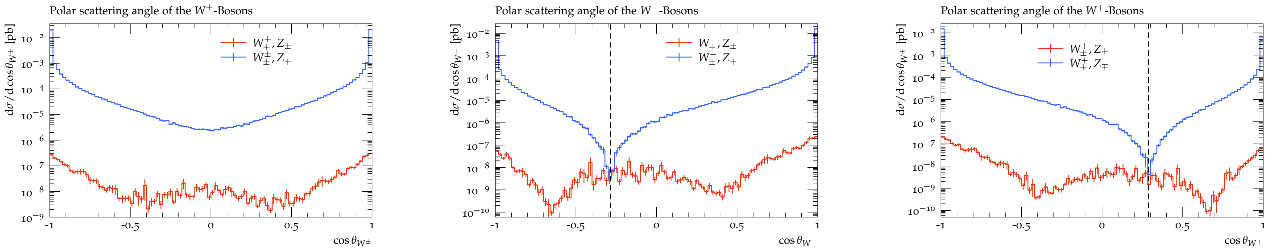

(a) (b) (c)

Figure 13: Histograms for the distribution of $\cos\theta$ of $W^\pm$- (a), W^-- (b) and W^+-bosons (c) in the $W^\pm Z$-production process in lepton-neutrino collisions for polarization combinations $\pm\pm$, $\pm\mp$ in lepton-neutrino collisions at $\sqrt{s} = 13$ TeV. The black dashed line in (b) and (c) marks the RAZ.

Polarization	$\sigma/\sigma_{total}[\%]$
Total	100
W_0^-, Z_0	0.658
W_T^-, Z_0	0.057
W_0^-, Z_T	0.063
W_T^-, Z_T	99.224

(a) W^-Z-production; combined polarizations

Polarization	$\sigma/\sigma_{total}[\%]$
Total	100
W_0^+, Z_0	0.658
W_T^+, Z_0	0.055
W_0^+, Z_T	0.060
W_T^+, Z_T	99.229

(b) W^+Z-production; combined polarizations

Polarization	$\sigma/\sigma_{total}[\%]$
Total	100
W_+^-, Z_+	0.005
W_-^-, Z_+	76.316
W_0^-, Z_+	0.044
W_+^-, Z_-	22.900
W_-^-, Z_-	0.003
W_0^-, Z_-	0.019
W_+^-, Z_0	0.019
W_-^-, Z_0	0.039
W_0^-, Z_0	0.658

(c) W^-Z-production; all polarizations

Polarization	$\sigma/\sigma_{total}[\%]$
Total	100
W_+^+, Z_+	0.003
W_-^+, Z_+	22.895
W_0^+, Z_+	0.019
W_+^+, Z_-	76.326
W_-^+, Z_-	0.004
W_0^+, Z_-	0.041
W_+^+, Z_0	0.037
W_-^+, Z_0	0.018
W_0^+, Z_0	0.658

(d) W^+Z-production; all polarizations

Table 3.4: Fractions of the cross-sections for both the W^-Z- and W^+Z-production in lepton-neutrino collisions for both the combined polarization states TT, TL, LT, LL and all polarization states at $\sqrt{s} = 13$ TeV.

4 Conclusion and Outlook

The goal of this thesis is to investigate if Sherpa is able to correctly simulate the effects of the polarization of $W^{\pm}$- and Z-bosons. One way is to study the existence of the theoretical RAZ effect in $W^{\pm}Z$-production and compare the results from Sherpa with the results from MadGraph which is already widely used in ATLAS. The results of both event generators are found to be very similar in all three simulated setups. In the 0J setup, the RAZ effect showed up. In the other two setups, the 1J and 0+1J setups, the RAZ effect did not show up. Since the analyzed process is simulated in an LHC setup, the RAZ effect cannot be seen like in a theoretical setup. At the LHC, there are many quantum mechanical effects which perturb the actual hard process. To observe the RAZ effect on a theoretical level, all settings in Sherpa which allow to simulate effects below the hard process have to be turned off. This effect is then investigated in fixed-parton and lepton-neutrino collisions. Those processes show the theoretical zeroes expected from analytical simulations at the expected scattering angle of the W^{-}- or W^{+}-bosons.

A very decisive evidence that the new Sherpa module works in the $W^{\pm}Z$-production in proton-proton collisions is by comparing the gathered results to the data of Run 3 of the LHC. Since the new Sherpa module also works for photons, another way of testing it, is in the $W^{\pm}\gamma$-production where the RAZ effect also appears. Right now however, the polarization of photons can only be simulated if the photon is not a part of the final state.

In the fixed-parton collisions, the RAZ is found at the four simulated center of mass energies $\sqrt{s} \in \{400\text{ GeV}, 2\text{ TeV}, 13\text{ TeV}, 200\text{ TeV}\}$. The only polarization combination of the $W^{\pm}$-bosons where the effect appears is $\pm\mp$ as predicted by the analytical calculations. For $\sqrt{s} \in \{2\text{ TeV}, 13\text{ TeV}, 200\text{ TeV}\}$, the RAZ is at the same scattering angle. For $\sqrt{s} = 400$ GeV on the other hand, the RAZ is almost at the same scattering angle as the other three simulated energies but not exactly since the absolute value of the momenta of the outgoing $W^{\pm}$- and Z-bosons is very close to the threshold where Eq. 12 cannot be approximated with Eq. 14 anymore.

The $W^{\pm}Z$-production in lepton-neutrino collisions at $\sqrt{s} = 13$ TeV also shows the RAZ at the expected scattering angle. If the other, in the fixed-parton collisions simulated, energies would be used to generate events for the lepton-neutrino collisions, the RAZ would appear just as in the fixed-parton collisions, since the only variables to change the scattering angle of the RAZ are the charges of the used fermions.

Bibliography

[1] Sherpa Team. *Sherpa Homepage*. https://sherpa-team.gitlab.io. Accessed: 2024-02-08.

[2] MG5aMC@NLO Development team. *The MadGraph5_ aMC@NLO homepage*. http://madgraph.phys.ucl.ac.be/. Accessed: 2024-02-08.

[3] Mareen Hoppe, Marek Schönherr, and Frank Siegert. *Polarised cross sections for vector boson production with SHERPA*. 2023. arXiv: 2310.14803 [hep-ph].

[4] Sandbox Studio. *Standard Model of particle physics*. https://www.energy.gov/science/doe-explainsthe-standard-model-particle-physics. Accessed: 2024-01-24.

[5] S. P. Martin and J. D. Wells. *Elementary Particles and Their Interactions*. First Edition. Springer, 2022. DOI: https://doi.org/10.1007/978-3-031-14368-7.

[6] G. Kane. *Modern Elementary Particle Physics: Explaining and Extending the Standard Model*. Second Edition. Cambridge University Press, 2017. DOI: https://doi.org/10.1017/9781316691434.

[7] Particle Data Group. *The Review of Particle Physics*. https://pdglive.lbl.gov/Viewer.action. Accessed: 2024-01-24. 2023.

[8] Sheldon L. Glashow. „The renormalizability of vector meson interactions“. In: *Nuclear Physics* 10 (1959), pp. 107–117. ISSN: 0029-5582. DOI: https://doi.org/10.1016/0029-5582(59)90196-8. URL: https://www.sciencedirect.com/science/article/pii/0029558259901968.

[9] A. Salam and J.C. Ward. „Weak and electromagnetic interactions“. In: *Nuovo Cim* 11 (1959), 568–577. DOI: https://doi.org/10.1007/BF02726525.

[10] Steven Weinberg. „A Model of Leptons“. In: *Phys. Rev. Lett.* 19 (21), pp. 1264–1266. DOI: 10.1103/PhysRevLett.19.1264. URL: https://link.aps.org/doi/10.1103/PhysRevLett.19.1264.

[11] M. Thomson. *Modern Particle Physics*. First Edition. Cambridge Univerity Press, 2013. DOI: https://doi.org/10.1017/CBO9781139525367.

[12] Andy Buckley et al. „General-purpose event generators for LHC physics“. In: *Physics Reports* 504.5 (2011), pp. 145–233. ISSN: 0370-1573. DOI: https://doi.org/10.1016/j.physrep.2011.03.005. URL: https://www.sciencedirect.com/science/article/pii/S0370157311000846.

[13] Enrico Bothmann et al. „Event generation with Sherpa 2.2“. In: *SciPost Phys.* 7 (2019), p. 034. DOI: 10.21468/SciPostPhys.7.3.034. URL: https://scipost.org/10.21468/SciPostPhys.7.3.034.

[14] Enrico Bothmann et al. „Event Generation with Sherpa 2.2“. In: *SciPost Phys.* 7.3 (2019), p. 034. DOI: 10.21468/SciPostPhys.7.3.034. arXiv: 1905.09127 [hep-ph].

[15] CERN. *The large hadron collider.* https://home.cern/science/accelerators/large-hadron-collider. Accessed: 2024-01-24. 2024.

[16] Sherpa Team. *Figure of the visualisation of a parcticle collision in Sherpa.* https://sherpa-team.gitlab.io/monte-carlo.html. Accessed: 2024-01-25.

[17] Sherpa Team. *Sherpa 3.0.0 Manual.* https://sherpa-team.gitlab.io/sherpa/master/index.html. Accessed: 2024-01-25.

[18] U. Baur, T. Han, and J. Ohnemus. „Amplitude zeros in $W^{\pm}$Z production“. In: *Phys. Rev. Lett.* 72 (25 1994), pp. 3941–3944. DOI: 10.1103/PhysRevLett.72.3941. URL: https://link.aps.org/doi/10.1103/PhysRevLett.72.3941.

[19] D. Decamp et al. „Measurement of the charged particle multiplicity distribution in hadronic Z decays“. In: *Phys. Lett. B* 273 (1991), pp. 181–192. DOI: 10.1016/0370-2693(91)90575-B.

[20] J. Alwall et al. „The automated computation of tree-level and next-to-leading order differential cross sections, and their matching to parton shower simulations“. In: *Journal of High Energy Physics* 2014.7 (July 2014). ISSN: 1029-8479. DOI: 10.1007/jhep07(2014)079. URL: http://dx.doi.org/10.1007/JHEP07(2014)079.

[21] Mareen Hoppe. *Implementation and phenomenology of polarized cross sections in the simulation of vector boson production with the SHERPA event generator.* https://cds.cern.ch/record/2872971?ln=en. 2023.

[22] Prachi Arvind Atmasiddha. *ATLAS_ WZ_ 00enhanced_ emu_ latest.cc.* https://gitlab.cern.ch/patmasid/rivetroutine_wz_00enhancedregion/-/blob/master/ATLAS_WZ_00enhanced_emu_latest.cc.

[23] Prachi Arvind Atmasiddha. *Observations of the Radiation Amplitude Zero effect and of the Diboson Longitudinal-Longitudinal Interactions in High pT Region using W±Z Production with the ATLAS Detector.* https://cernbox.cern.ch/s/3lEpyDsv2ixbxMX. 2023.

[24] Hepforge. *Rivet — the particle-physics MC analysis toolkit.* https://rivet.hepforge.org/. Accessed: 2024-02-03.

[25] D. Berdine, N. Kauer, and D. Rainwater. „Breakdown of the Narrow Width Approximation for New Physics". In: *Phys. Rev. Lett.* 99 (11 2007), p. 111601. DOI: 10.1103/PhysRevLett.99.111601. URL: https://link.aps.org/doi/10.1103/PhysRevLett.99.111601.

[26] J. C. Ward. „An Identity in Quantum Electrodynamics". In: *Phys. Rev.* 78 (2 1950), pp. 182–182. DOI: 10.1103/PhysRev.78.182. URL: https://link.aps.org/doi/10.1103/PhysRev.78.182.

[27] Particle Data Group. *Monte Carlo Particle Numbering Scheme.* https://pdg.lbl.gov/2009/mcdata/mc_particle_id_contents.html. 2009.

A Selbstständigkeitserklärung

Hiermit versichere ich, dass ich, Johannes Nikolas Liebig, die vorliegende Bachelorarbeit im Rahmen der Betreuung am Institut für Kern- und Teilchenphysik selbstständig verfasst habe und keine anderen als die angegebenen Quellen und Hilfsmittel benutzt sowie Zitate kenntlich gemacht habe.
Diese Arbeit wurde noch nicht in gleicher oder ähnlicher Form im Rahmen einer anderen Prüfungsleistung vorgelegt.

Johannes Nikolas Liebig
Dresden, den 12. Februar 2024

B Run-cards

In this part of the appendix, the used run-cards are displayed. Since many run-cards were used, they are shown modular.
For the processes on proton level, the general run-card set-up is seen in B.1 with the possible options in tables B.1, B.2 and B.3.
For the processes on fixed-parton level and with leptons, the general run-card set-up is seen in B.2 with the viable options in tables B.4, B.5 and B.6.

Listing B.1: run-card for W+/- Z production for 0J at proton level

```
BEAMS: 2212
BEAM_ENERGIES: 6500
HEPMC_USE_NAMED_WEIGHTS: 1
ME_GENERATORS:
    - Comix
    - Amegic
    - OpenLoops
PDF_LIBRARY: LHAPDFSherpa
PDF_SET: NNPDF30_nlo_as_0118
MEPS:
    CORE_SCALE: VAR{0.25*Abs2(p[2]+p[3])}
COMIX_DEFAULT_GAUGE: 0
PROCESSES: (1*) (1**)
    - 93 93 -> 24 23:
        Order: {QCD: 0, EW: 2}
PARTICLE_DATA:
    24: {Width: 0}
    23: {Width: 0}
WIDTH_SCHEME: Fixed
HARD_DECAYS:
    Enabled: true
    Channels: (1***)
        24,12,-11: {Status: 2}
        24,14,-13: {Status: 2}
```

```
        23,11,-11: {Status: 2}
        23,13,-13: {Status: 2}
    Pol_Cross_Section:
        Enabled: true
        Reference_System: [Lab, COM]
ANALYSIS: Rivet
RIVET:
  --analyses:
    - MC_WZRAZ
```

W^+Z-production	W^-Z-production
- 93 93 -> 24 23	-93 93 -> -24 23

Table B.1: (1*) Sherpa settings for the different simulated processes [17]. The corresponding PIDs can be looked up in Ref. [27].

0J	1J	0+1J
Order: {QCD: 0, EW: 2}	Order: {QCD: 0, EW: 2} CKKW: 20	Order: {QCD: 1, EW: 2} SELECTORS: - NJetFinder: N: 1 PTMin: 5.0 Exp: -1

Table B.2: (1**) Sherpa settings for different amount of jets [17].

W^+Z-production	W^-Z-production
24,12,-11: {Status: 2}	-24,-12,11: {Status: 2}
24,14,-13: {Status: 2}	-24,-14,13: {Status: 2}
23,11,-11: {Status: 2}	23,11,-11: {Status: 2}
23,13,-13: {Status: 2}	23,13,-13: {Status: 2}

Table B.3: (1***) Sherpa settings for hard decays [17]. The corresponding PIDs can be looked up in Ref. [27].

Listing B.2: run-card for a fixed-parton collision to produce W+ and Z

```
MI_HANDLER: None
SHOWER_GENERATOR: None
FRAGMENTATION: None
ME_QED: {ENABLED: false}
BEAM_REMNANTS: false
YFS:
```

```
    MODE: None
BEAMS: [2, -1] (2*)
BEAM_ENERGIES: [6500, 6500] (2**)
HEPMC_USE_NAMED_WEIGHTS: 1
ME_GENERATORS:
    - Comix
    - Amegic
    - OpenLoops
SCALES: VAR{0.25*Abs2(p[2]+p[3])}
COMIX_DEFAULT_GAUGE: 0
PROCESSES:
    - 2 -1 -> 24 23: (2***)
        Order: {QCD: 0, EW: 2}
PARTICLE_DATA:
    24: {Width: 0}
    23: {Width: 0}
WIDTH_SCHEME: Fixed
HARD_DECAYS:
    Enabled: true
    Channels:
        24,12,-11: {Status: 2}
        24,14,-13: {Status: 2}
        23,11,-11: {Status: 2}
        23,13,-13: {Status: 2}
    Pol_Cross_Section:
        Enabled: true
        Reference_System: [Lab, COM]
    QED_Corrections: 0
ANALYSIS: Rivet
RIVET:
  --analyses:
    - MC_WZRAZ_more_bins
  --ignore-beams: 1
```

$u+\bar{d} \to W^+ + Z$	$d+\bar{u} \to W^- + Z$	$\nu_e + e^+ \to W^+ + Z$	$e^- + \overline{\nu_e} \to W^- + Z$
BEAMS: [2, -1]	BEAMS: [1, -2]	BEAMS: [-11, 12]	BEAMS: [11, -12]

Table B.4: (2*) Sherpa settings for the different beam setups [17]. The corresponding PIDs can be looked up in Ref. [27].

$\sqrt{s}$ = 400 GeV	BEAM_ENERGIES: [200, 200]
$\sqrt{s}$ = 2 TeV	BEAM_ENERGIES: [1000, 1000]
$\sqrt{s}$ = 13 TeV	BEAM_ENERGIES: [6500, 6500]
$\sqrt{s}$ = 200 TeV	BEAM_ENERGIES: [100000, 100000]

Table B.5: (2**) Sherpa settings for different center of mass energies using two beams [17].

$u+\overline{d} \to W^+ + Z$	$d+\overline{u} \to W^- + Z$	$\nu_e + e^+ \to W^+ + Z$	$e^- + \overline{\nu_e} \to W^- + Z$
2 -1 -> 24 23	1 -2 -> -24 23	-11 12 -> 24 23	11 -12 -> -24 23

Table B.6: (2***) Sherpa process settings the different beam setups [17]. The corresponding PIDs can be looked up in Ref. [27].

C Graphs

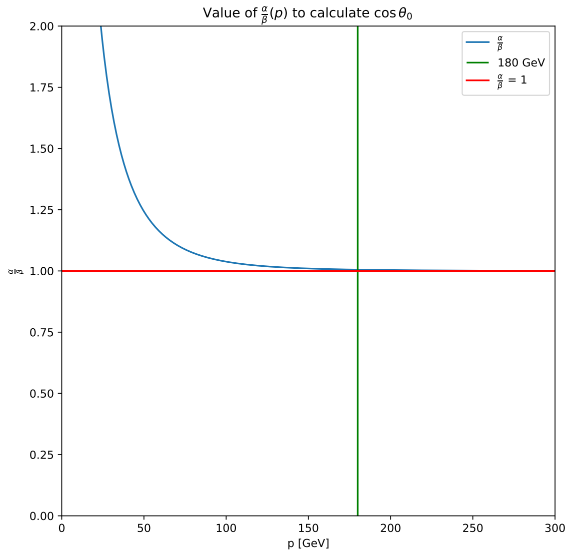

Figure C.1: The function $\frac{\alpha}{\beta}(p)$ to derive Eq. 14 from Eq. 12.

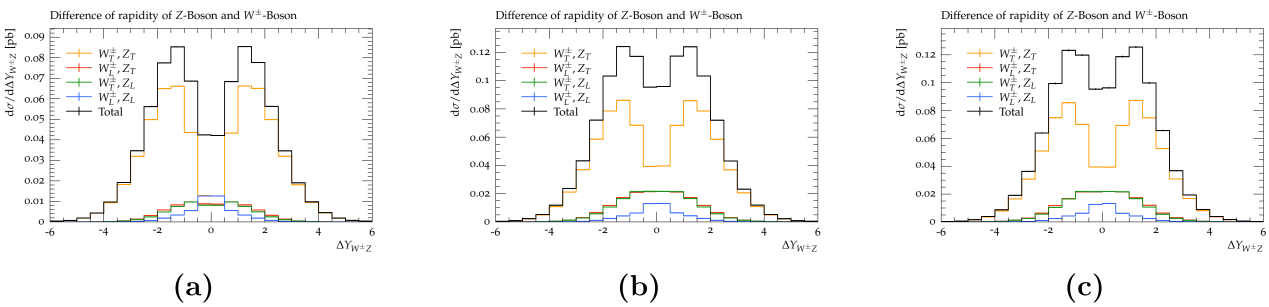

Figure C.2: Rapidity difference between W$^{\pm}$- and Z-boson in the $W^{\pm}Z$-production process in proton-proton collisions at $\sqrt{s} = 13$ TeV for the setups 0J (a), 1J (b) and 0+1J (c).

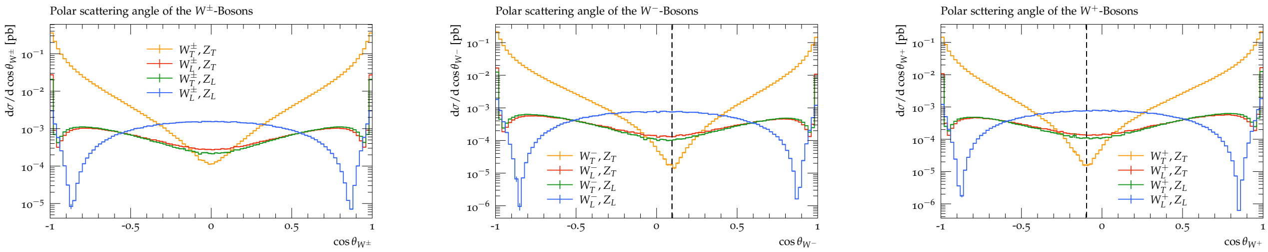

(a) **(b)** **(c)**

Figure C.3: Distributions of $\cos\theta$ of $W^\pm$ (a), W^- (b) and W^+ (c) in the $W^\pm Z$-production process in fixed-parton collisions for the polarization combinations TT, TL, LT and LL at $\sqrt{s} = 400$ GeV. The black dashed line in (b) and (c) marks the RAZ.

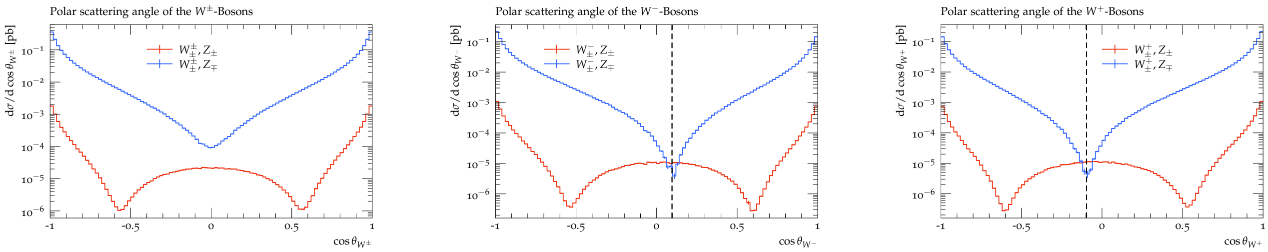

(a) **(b)** **(c)**

Figure C.4: Distributions of $\cos\theta$ of $W^\pm$ (a), W^- (b) and W^+ (c) in the $W^\pm Z$-production process in fixed-parton collisions for the polarization combinations $\pm\pm$ and $\pm\mp$ at $\sqrt{s} = 400$ GeV. The black dashed line in (b) and (c) marks the RAZ.

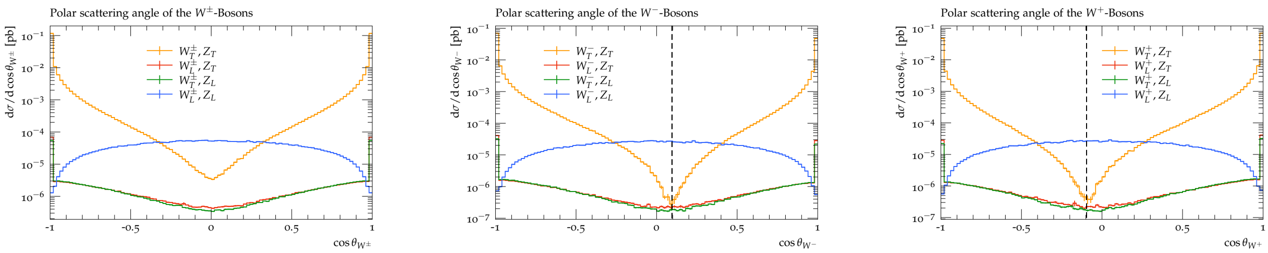

(a) **(b)** **(c)**

Figure C.5: Distributions of $\cos\theta$ of $W^\pm$ (a), W^- (b) and W^+ (c) in the $W^\pm Z$-production process in fixed-parton collisions for the polarization combinations TT, TL, LT and LL at $\sqrt{s} = 2$ TeV. The black dashed line in (b) and (c) marks the RAZ.

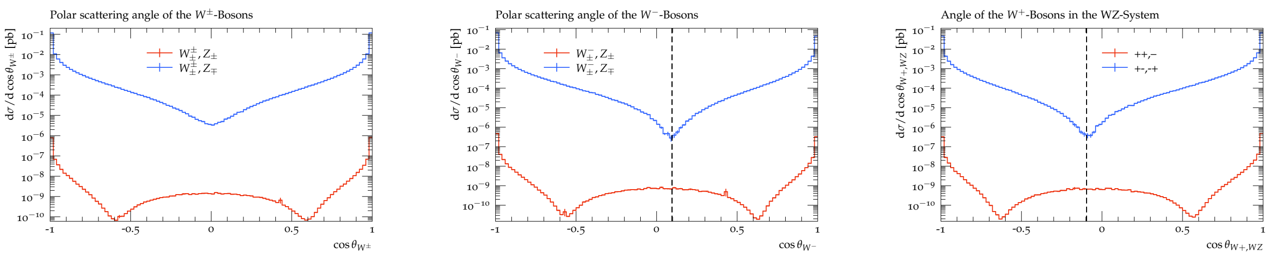

(a) **(b)** **(c)**

Figure C.6: Distributions of $\cos\theta$ of $W^\pm$ (a), W^- (b) and W^+ (c) in the $W^\pm Z$-production process in fixed-parton collisions for the polarization combinations $\pm\pm$ and $\pm\mp$ at $\sqrt{s} = 2$ TeV. The black dashed line in (b) and (c) marks the RAZ.

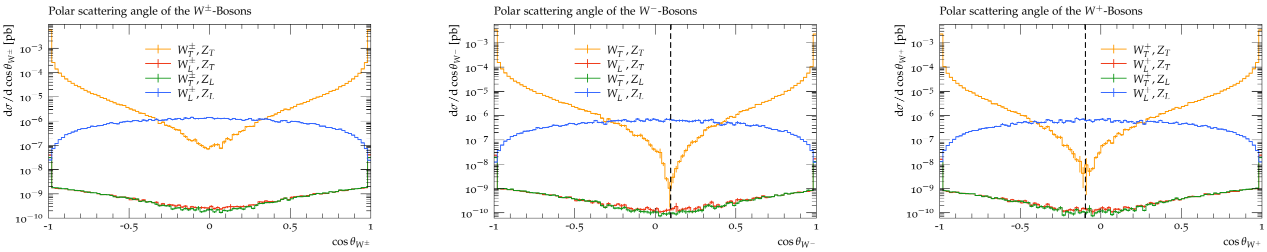

(a) (b) (c)

Figure C.7: Distributions of $\cos\theta$ of W$^{\pm}$ (a), W^{-} (b) and W^{+} (c) in the $W^{\pm}Z$-production process in fixed-parton collisions for the polarization combinations TT, TL, LT and LL at $\sqrt{s} = 13$ TeV. The black dashed line in (b) and (c) marks the RAZ.

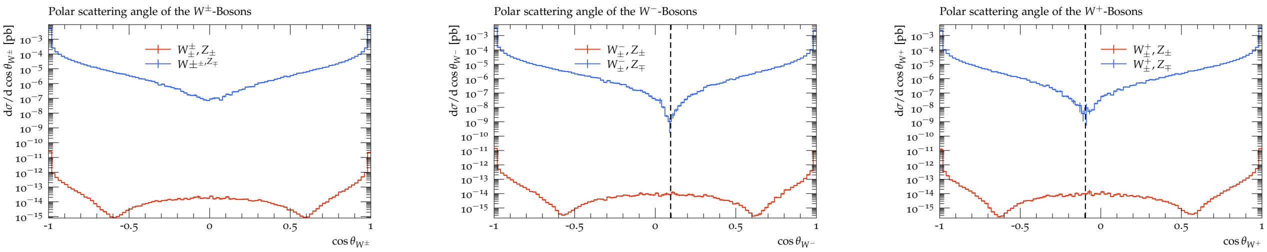

(a) (b) (c)

Figure C.8: Distributions of $\cos\theta$ of W$^{\pm}$ (a), W^{-} (b) and W^{+} (c) in the $W^{\pm}Z$-production process in fixed-parton collisions for the polarization combinations $\pm\pm$ and $\pm\mp$ a $\sqrt{s} = 13$ TeV. The black dashed line in (b) and (c) marks the RAZ.

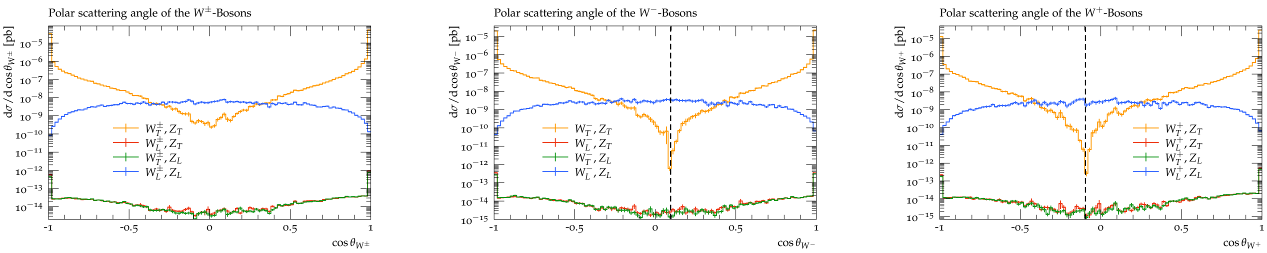

(a) (b) (c)

Figure C.9: Distributions of $\cos\theta$ of W$^{\pm}$ (a), W^{-} (b) and W^{+} (c) in the $W^{\pm}Z$-production process in fixed-parton collisions for the polarization combinations TT, TL, LT and LL at $\sqrt{s} = 200$ TeV. The black dashed line in (b) and (c) marks the RAZ.

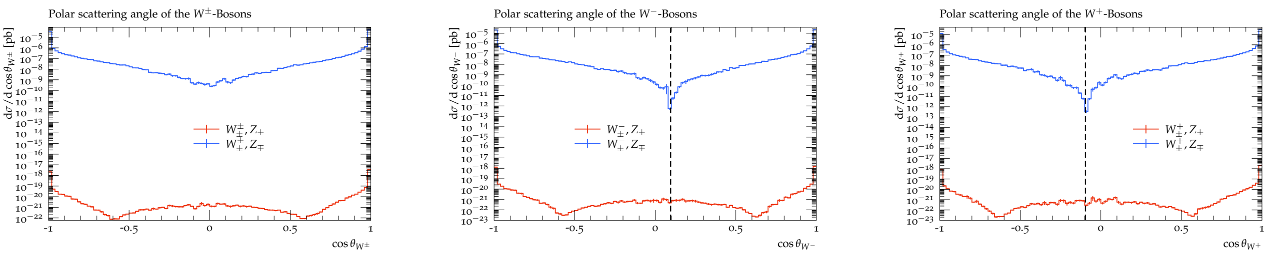

(a) (b) (c)

Figure C.10: Distributions of $\cos\theta$ of W$^{\pm}$ (a), W^{-} (b) and W^{+} (c) in the $W^{\pm}Z$-production process in fixed-parton collisions for the polarization combinations $\pm\pm$ and $\pm\mp$ at $\sqrt{s} = 200$ TeV. The black dashed line in (b) and (c) marks the RAZ.

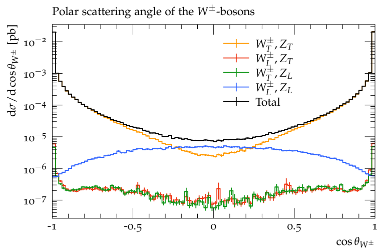

Figure C.11: Distribution of $\cos\theta$ of W$^{\pm}$ in the $W^{\pm}Z$-production process in lepton-neutrino collisions for the polarization combinations TT, LT, TL and LL at $\sqrt{s} = 13$ TeV.

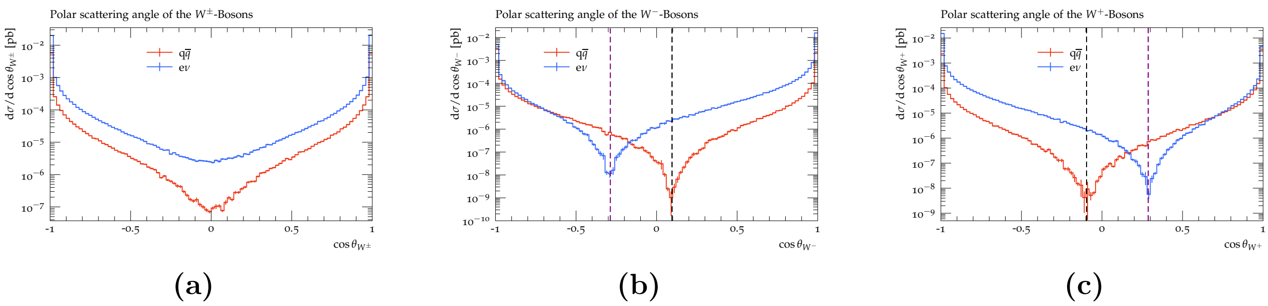

Figure C.12: Comparison of the distributions of $\cos\theta$ of W$^{\pm}$ (a), W^{-} (b) and W^{+} (c) in the $W^{\pm}Z$-production process for polarization TT in fixed-parton and lepton-neutrino collisions at $\sqrt{s} = 13$ TeV. The theoretical zero predicted by the RAZ is marked as the black dashed line for fixed-parton collisions and as the purple dashed line for lepton-neutrino collisions.

D Tables

Polarization	$\sigma/\sigma_{total}[\%]$
Total	100
W^-_+, Z_+	0.173
W^-_-, Z_+	35.048
W^-_0, Z_+	1.743
W^-_+, Z_-	53.712
W^-_-, Z_-	0.192
W^-_0, Z_-	2.330
W^-_+, Z_0	2.039
W^-_-, Z_0	1.571
W^-_0, Z_0	3.238

(a) $\sqrt{s}\ =\ 400$ GeV

Polarization	$\sigma/\sigma_{total}[\%]$
Total	100
W^-_+, Z_+	0.000
W^-_-, Z_+	39.651
W^-_0, Z_+	0.037
W^-_+, Z_-	59.068
W^-_-, Z_-	0.000
W^-_0, Z_-	0.049
W^-_+, Z_0	0.043
W^-_-, Z_0	0.033
W^-_0, Z_0	1.118

(b) $\sqrt{s}\ =\ 2$ TeV

Polarization	$\sigma/\sigma_{total}[\%]$
Total	100
W^-_+, Z_+	0.000
W^-_-, Z_+	40.054
W^-_0, Z_+	0.001
W^-_+, Z_-	59.313
W^-_-, Z_-	0.000
W^-_0, Z_-	0.001
W^-_+, Z_0	0.001
W^-_-, Z_0	0.000
W^-_0, Z_0	0.628

(c) $\sqrt{s}\ =\ 13$ TeV

Polarization	$\sigma/\sigma_{total}[\%]$
Total	100
W^-_+, Z_+	0.000
W^-_-, Z_+	51.381
W^-_0, Z_+	0.000
W^-_+, Z_-	48.174
W^-_-, Z_-	0.000
W^-_0, Z_-	0.000
W^-_+, Z_0	0.000
W^-_-, Z_0	0.000
W^-_0, Z_0	0.443

(d) $\sqrt{s}\ =\ 200$ TeV

Table D.1: Fractions of the cross-sections for the W^-Z-production in fixed-parton collisions of all polarization states for different center of mass energies. When $\sigma\ =\ 0.0$ in the table, the cross-section is very low, but non-zero.

Polarization	$\sigma/\sigma_{total}[\%]$
Total	100
W_0^+, Z_0	3.228
W_T^+, Z_0	3.605
W_0^+, Z_T	4.056
W_T^+, Z_T	89.110

(a) $\sqrt{s}$ = 400 GeV

Polarization	$\sigma/\sigma_{total}[\%]$
Total	100
W_0^+, Z_0	1.119
W_T^+, Z_0	0.076
W_0^+, Z_T	0.086
W_T^+, Z_T	98.716

(b) $\sqrt{s}$ = 2 TeV

Polarization	$\sigma/\sigma_{total}[\%]$
Total	100
W_0^+, Z_0	0.629
W_T^+, Z_0	0.001
W_0^+, Z_T	0.001
W_T^+, Z_T	99.368

(c) $\sqrt{s}$ = 13 TeV

Polarization	$\sigma/\sigma_{total}[\%]$
Total	100
W_0^+, Z_0	0.420
W_T^+, Z_0	0.000
W_0^+, Z_T	0.000
W_T^+, Z_T	99.586

(d) $\sqrt{s}$ = 200 TeV

Table D.2: Fractions of the cross-sections for the W^+Z-production in fixed-parton collisions of the combined polarization states TT, TL, LT, LL for different center of mass energies.

Polarization	$\sigma/\sigma_{total}[\%]$
Total	100
W^+_+, Z_+	0.193
W^+_-, Z_+	53.695
W^+_0, Z_+	2.315
W^+_+, Z_-	35.055
W^+_-, Z_-	0.174
W^+_0, Z_-	1.741
W^+_+, Z_0	1.568
W^+_-, Z_0	2.038
W^+_0, Z_0	3.228

(a) $\sqrt{s}$ = 400 GeV

Polarization	$\sigma/\sigma_{total}[\%]$
Total	100
W^+_+, Z_+	0.000
W^+_-, Z_+	59.056
W^+_0, Z_+	0.049
W^+_+, Z_-	39.659
W^+_-, Z_-	0.000
W^+_0, Z_-	0.037
W^+_+, Z_0	0.033
W^+_-, Z_0	0.043
W^+_0, Z_0	1.119

(b) $\sqrt{s}$ = 2 TeV

Polarization	$\sigma/\sigma_{total}[\%]$
Total	100
W^+_+, Z_+	0.000
W^+_-, Z_+	59.262
W^+_0, Z_+	0.001
W^+_+, Z_-	40.107
W^+_-, Z_-	0.000
W^+_0, Z_-	0.000
W^+_+, Z_0	0.000
W^+_-, Z_0	0.001
W^+_0, Z_0	0.629

(c) $\sqrt{s}$ = 13 TeV

Polarization	$\sigma/\sigma_{total}[\%]$
Total	100
W^+_+, Z_+	0.000
W^+_-, Z_+	69.559
W^+_0, Z_+	0.000
W^+_+, Z_-	30.024
W^+_-, Z_-	0.000
W^+_0, Z_-	0.000
W^+_+, Z_0	0.000
W^+_-, Z_0	0.000
W^+_0, Z_0	0.420

(d) $\sqrt{s}$ = 200 TeV

Table D.3: Fractions of the cross-sections for the W^+Z-production in fixed-parton collisions of all polarization states for different center of mass energies. When $\sigma = 0.0$ in the table, the cross-section is very low, but non-zero.